ISTANBUL TECHNICAL UNIVERSITY ★ GRADUATE SCHOOL

SYNTHESIS AND CHARACTERISATION OF PBI MEMBRANES FOR HT-PEM FUEL CELLS

M.Sc. THESIS

Mehmet Turan GÖRÜRYILMAZ

Energy Science and Technology Division

Energy Science and Technology Programme

JULY 2021

ISTANBUL TECHNICAL UNIVERSITY ★ GRADUATE SCHOOL

SYNTHESIS AND CHARACTERISATION OF PBI MEMBRANES FOR HT-PEM FUEL CELLS

M.Sc. THESIS

Mehmet Turan GÖRÜRYILMAZ
(301171045)

Energy Science and Technology Division

Energy Science and Technology Programme

Thesis Advisor: Prof. Dr. Nilgün KARATEPE YAVUZ
Thesis Co-Advisor: Dr. Sibel ÖZENLER

JULY 2021

İSTANBUL TEKNİK ÜNİVERSİTESİ ★ LİSANSÜSTÜ EĞİTİM ENSTİTÜSÜ

HT-PEM YAKIT HÜCRELERİ İÇİN PBI MEMBRAN SENTEZİ VE KARAKTERİZASYONU

YÜKSEK LİSANS TEZİ

Mehmet Turan GÖRÜRYILMAZ
(301171045)

Enerji Bilim ve Teknoloji Anabilim Dalı

Enerji Bilim ve Teknoloji Programı

Tez Danışmanı: Prof. Dr. Nilgün KARATEPE YAVUZ
Eş Danışman: Dr. Sibel ÖZENLER

TEMMUZ 2021

Mehmet Turan GÖRÜRYILMAZ, a M.Sc. student of İTU Graduate School student ID 301171045 successfully defended the thesis entitled "SYNTHESIS AND CHARACTERISATION OF PBI MEMBRANES FOR HT-PEM FUEL CELLS", which he prepared after fulfilling the requirements specified in the associated legislations, before the jury whose signatures are below.

Thesis Advisor :	**Prof. Dr. Nilgün KARATEPE YAVUZ** Istanbul Technical University	.....
Co-advisor :	**Dr. Sibel ÖZENLER** Turkish - German University	.....
Jury Members :	**Prof. Dr. Ayfer KALKAN BURAT** Istanbul Technical University	.....
	Assoc. Prof. Dr. Bihter ZEYTUNCU GÖKOĞLU Istanbul Technical University	.....
	Assoc. Prof. Dr. GÖKÇEN ALTUN ÇİFTÇİOĞLU Marmara University	.....

Date of Submission : 23 June 2021
Date of Defense : 11 July 2021

To my family,

FOREWORD

First of all, I would like to thank my advisor Prof. Dr. Nilgün K. YAVUZ for agreeing to work with me and my co-advisor Dr. Sibel ÖZENLER for her help along the way.

I also thank Assoc. Prof. Dr. Bihter ZEYTUNCU GÖKOĞLU for her help with the polymer synthesis, as well as FT-IR and SEM analyses. I was always able to reach her comfortably.

I thank Prof. Dr. Ayfer K. BURAT for her help with the NMR analysis.

I thank PhD candidate Zeynep ERDÖL for her help with every laboratory related topic I asked her and for sharing her knowledge on EIS with me.

I thank PhD candidate Şanser ÇELENK for his help on the HT-PEM subject.

Finally, I thank my parents for giving me every possible support that they can.

I am indebted to ITU BAP for their financial support in this study under the project code MYL-2019-42464.

June 2021

Mehmet Turan GÖRÜRYILMAZ
(Mechanical Engineer)

TABLE OF CONTENTS

Page

ABBREVIATIONS

AC	**:** Alternative Current
AFC	**:** Alkaline Fuel Cell
BI	**:** Benzimidazole
C	**:** Capacitance
CV	**:** Cyclic Voltammetry
CPE	**:** Constant Phase Element
DAB	**:** Diaminobenzidine
DC	**:** Direct Current
DI	**:** De-ionised
DMAc	**:** Dimethylacetamide
EIS	**:** Electrochemical Impedance Spectroscopy
FT-IR	**:** Fourier Transform Infrared Spectroscopy
GO	**:** Graphene Oxide
m-PBI	**:** m-polybenzimidazole (poly [2,2'-(m-phenylene)-5,5'-bibenzimidazole])
MCFC	**:** Molten Carbonate Fuel Cell
MWCNT	**:** Multi-walled Carbon Nanotube
NMR	**:** Nuclear Magnetic Resonance
IPA	**:** Isophthalic Acid
OCV	**:** Open Circuit Voltage
PA	**:** Phosphoric Acid
PAFC	**:** Phosphoric Acid Fuel Cell
PBI	**:** Polybenzimidazole
PEM	**:** Proton Exchange (or Polymer Electrolyte) Membrane
PEMFC	**:** PEM Fuel Cell
PPA	**:** Polyphosphoric Acid
PTFE	**:** Polytetrafluoroethylene, Teflon
SOFC	**:** Solid Oxide Fuel Cell
TG	**:** Thermogravimetry

SYMBOLS

a_c	: Catalyst Specific Area (cm^2/mg)
A	: Pre-exponential Factor
D	: The distance between the electrodes
E	: The theoretical cell potential (V)
E_a	: Activation energy for proton transfer (J/mol)
E_c	: Activation energy for O2 reduction on the catalyst (J/mol)
E_{cell}	: Cell potential (V)
$E_{Polarisation}$	: Potential losses (V)
F	: The Faraday's Constant (96,485 C/mol)
G	: Gibbs Free Energy
H	: Hydrogen
H	: Enthalpy (Joule)
i	: Current Density
i_0	: Exchange Current Density (A/cm^2 Pt)
L_c	: Catalyst Loading (mg Pt/cm^2)
l_m	: Membrane length
M_W	: Molecular Weight (gr/mol)
n	: Number of electrons per molecule of H_2
N_{Avg}	: Avogadro's Number
P	: Pressure
Pa	: Pascal
Pd	: Palladium
P_r	: Reactant partial pressure (kPa)
Pt	: Platin
q	: Charge (coulombs/mol)
q_{el}	: Charge of 1 electron
R	: Resistance (ohm)
R	: Ideal Gas Constant (8.314 J/molK)
S	: Entropy (Joule)
T	: Temperature

$\mathbf{t_m}$: Membrane Thickness

V : Volt

$\mathbf{V_m}$: Molar Volume

W : Watt

$\mathbf{W_{el}}$: Electrical Work

$\mathbf{w_m}$: Membrane width

Z : Impedance

α : Transfer coefficient

Δ : Change

γ : Pressure Coefficient

η : Efficiency

$\boldsymbol{\eta_{int}}$: Intrinsic Viscosity (dl/g)

λ : Wavelenght (Å)

σ : Conductivity (S/cm)

LIST OF TABLES

Page

LIST OF FIGURES

Page

SYNTHESIS AND CHARACTERISATION OF PBI MEMBRANES FOR HT-PEM FUEL CELLS

SUMMARY

In recent years, more and more researches are being done on the fuel cells. Improving the components of the cell is progressively advancing. One of these research subjects is the membrane technology. Polybenzimidazole (PBI) membranes are suitable in fuel cell uses, like the Nafion membranes, due to their thermal stability, high mechanical strength and protonic conductivity. One of the advantages of the PBI membranes is that they do not depend on humidity like Nafion membranes.

In this study, PBI membranes for high temperature fuel cells (HT-PEMFCs) were synthesised and tested. The polymer was synthesised according to solution polymerisation method. After that, the characterisation of the product was accomplished by using various instruments and methods, such as nuclear magnetic resonance (NMR) spectroscopy, thermogravimetry (TG) and fourier transform infrared spectroscopy (FT-IR). Then, the membranes were prepared by dissolving PBI polymer in DMAc and casted. At this step, different amounts of multi-walled carbon nanotubes (MWCNTs) were also added to the solutions. The undoped membranes were analysed by X-Ray diffraction (XRD). Then they were immersed into the phosphoric acid and doping procedure was conducted. Both doped and undoped membranes were characterised and compared by TGA, FT-IR and scanning electron microscopy (SEM). The protonic conductivity test of the doped membranes was carried out on electrochemical impedance spectroscopy.

NMR results showed that the synthesised polymer was indeed PBI, along with the TGA and FT-IR results. The doping levels were calculated as 14.3 mol PA/PBI for the pristine PBI, 5.9 mol PA/PBI for the 0.5wt% MWCNT/PBI membrane and 7.3 mol PA/PBI for the 1wt% MWCNT/PBI membrane. The conductivity tests were carried out under anhydrous conditions. Protonic conductivity at 120 °C, 140 °C and 160 °C for pristine PBI membrane were calculated as 0.0518 S/cm, 0.0667 S/cm and 0.0895 S/cm, respectively. The conductivities of the 0.5wt% PBI/MWCNT membrane were found as 0.0401 S/cm, 0.0586 S/cm and 0.0613 S/cm for 120 °C, 140 °C and 160 °C, respectively. For the 1wt% PBI/MWCNT membrane, slightly higher conductivities were obtained as 0.0429 S/cm, 0.0621 S/cm and 0.0655 S/cm for the temperatures 120 °C, 140 °C and 160 °C, respectively.

HT-PEM YAKIT HÜCRELERİ İÇİN PBI MEMBRAN SENTEZİ VE KARAKTERİZASYONU

ÖZET

Son yıllarda, yakıt pilleri konusunda yapılan çalışmalar gittikçe artmaktadır. Pillerin parçalarının geliştirilmesi adım adım ilerlemektedir. Bu araştırma alanlarından birisi de membran teknolojisidir. PEMYP genelde Nafyon membran kullanmaktadır ve çalışma sıcaklığı 80 °C'dir. Ancak bu düşük sıcaklık, düşük oksijen indirgeme kinetikleri, düşük ısı ve su yönetimi ve gaz safsızlığına karşı düşük tolerans yüzünden sorunlar oluşturmaktadır. Bu sebeple polibenzimidazol (PBI) membranlar tanıtılmıştır.

PBI membranlar, ısıl dayanımları, yüksek mukavemetleri ve protonik iletkenlikleri sebebiyle yakıt pilleri için Nafyon gibi uygun birer adaydır. Avantajlarından birisi de Nafyon gibi nem dengesine bağlı olmamalarıdır. Yüksek sıcaklıklarından dolayı, PBI membranlarda sıvı su oluşumu gözlenmez ve düşük bağıl nem sayesinde su yönetimine ihtiyaç duyulmaz.

PBI membranlar, yüksek sıcaklıklı proton değişim elemanlı yakıt pillerinde en yaygın kullanılan membran türüdür. 200 °C'ye kadar mükemmel ısıl dayanım gösterirler. Isıl gerilmelere karşı dayanıklılığı ve yüksek protonik iletkenliği, bu membranın tercih edilmesinde önemli rol oynar. Karbonlu destek yapıları eklenerek, bu membranların iyonik iletkenliklerinde ve mekanik dayanımlarında artış sağlanabilir. Grafen oksit ve karbon nanotüp desteği, bu alanda en yaygın olan kullanımlardır.

Bu çalışmada, yüksek sıcaklıklı polimer elektrolit membranlı yakıt pilleri (YS-PEMYP) için PBI membranlar sentezlenmiş ve test edilmiştir. Polimer, çözelti polimerleştirme yöntemine göre sentezlenmiştir. Öncelikle monomerler bir gece etüvde 80 °C'de kurutulmuş ve içlerindeki nem uzaklaştırılmıştır. Daha sonra 3 boyunlu dibi yuvarlak bir cam balon, yağ banyosuna oturtulmuş ve tepesine mekanik karıştırıcı bağlanmıştır. Kollardan biri azot girişi olarak azot tüpüne, diğeri ise azot çıkışı ve nem tutucu olarak kalsiyum klorür dolu bir U boruya bağlanmıştır. Belli bir miktar polifosforik asit, cam balon içine konmuş ve kuruması icin 140 °C'de 3 saat ısıtılmıştır. Daha sonra, içine ilk monomer olan diaminobenzidin tetrahidroklorit (DAB.4HCl) eklenmiş ve 2 saat boyunca HCl balonu kalmayana kadar mekanik olarak karıştırılmıştır. Bundan sonra, sıcaklık 170 °C'ye çıkartılmış, karıştırma hızı düşürülmüş ve DAB ile aynı molde izoftalik asit (IPA) balona eklenmiştir. 4.5 saat karıştırıldıktan sonra sıcaklık 200 °C'ye çıkartılmış ve 24 saat boyunca tepkime gerçekleşmiştir. 24 saat sonunda oluşan viskoz sıvı, oda sıcaklığındaki deiyonize suya dökülmüş ve çökelti şeklinde PBI lifleri elde edilmiştir. Bolca deiyonize su ile yıkanmış ve bir gece boyunca ağırlıkça %5'lik sodyum bikarbonat çözeltisi içinde mekanik olarak karıştırılmıştır. Daha sonra yine bolca deiyonize su ve metanol ile yıkanan PBI lifleri, bir gece boyunca 150 °C´de etüvde kurutulmuş ve öğütülerek PBI polimeri tozu elde edilmiştir.

Sentezlenen polimer, nükleer manyetik rezonans, termogravimetrik analiz ve fourier dönüşümlü kızılötesi spektroskopisi yöntemleriyle karakterize edilmiş ve sentezlenen

polimerin PBI olduğunu doğrulanmıştır. Nükleer manyetik rezonans testinde bütün karateristik tepe noktaları açıkça görülebilmektedir. Isıl dengeyi belirlemek amacıyla kullanılan termogravimetrik analiz testi, bozunma sıcaklığını 550 °C olarak göstermiştir. Fourier dönüşümlü kızılötesi spektroskopisi ise 4000-650 cm^{-1} arasında yapılmış ve karakteristik PBI değerlerini vermiştir.

Sonraki adımda, ağırlıkça %5'lik PBI polimeri, ağırlıkça %3'lük DMAc/LiCl karışımı içerisinde 2 saat boyunca 80 °C'de manyetik olarak karıştırılarak çözündürülmüş ve sonrasında 1 saat boyunca santrifüj edilerek membran çözeltileri elde edilmiştir. Bu adımda, farklı miktarlarda çok duvarlı karbon nanotüpler, hazırlanan çözeltilere eklenmiştir. Ağırlıkça %0.5 PBI/ÇDKNT ve ağırlıkça %1 PBI/ÇDKNT membran çözeltileri hazırlanmıştır. Daha sonra dökme yöntemiyle membranlar elde edilmiştir. Belirtilen miktarlardaki çok duvarlı karbon nanotüpler PBI/DMAc içinde 6 saat boyunca buz banyosunda ultrasonik olarak homojenize edilmişlerdir. Daha sonra çözeltiler etüvde bir gece boyunca 80 °C'de kurutularak membranlar elde edilmiştir. Elde edilen membranlar, LiCl'ü uzaklaştırmak için 5 saat kaynar deiyonize su içinde bekletilmiş, daha sonra tekrar etüv içinde 190 °C'de 3 saat boyunca hem su hem de kalan çözücü uzaklaştırılmıştır.

Katkılandırılmamış membranlar, X-ışını kırılması yöntemiyle analiz edilmişlerdir ve $2\theta = 25°$'de, PBI'ın yarı kristal yapısından dolayı tepe değeri vermişlerdir. Bu tepe değerinin yoğunluğu, artan çok duvarlı karbon nanotüp miktari ile artmaktadir.

Son olarak, membranlar fosforik asite batırılmış ve asit katkılama işlemi yürütülmüştür. Membranlara ait katkılama değerleri, saf PBI membran için 14.3 mol FA/PBI, ağırlıkça %0.5 PBI/ÇDKNT membran için 5.9 mol FA/PBI, ağırlıkça %1 PBI/ÇDKNT membran için ise mol 7.3 mol FA/PBI olarak hesaplanmıştır.

Daha sonra hem katkısız hem de katkılı membranlar TGA, FT-IR ve tarayıcı elektron mikroskopisi testlerine tabii tutulmuşlardır. TGA testinde membranlar, öğütülmüş polimer ile aynı bozunma sıcaklığına sahiptir. Kompozit membranlarda 220-420 °C arasında PBI kaplı ÇDKNTler bozunmaya başlamıştır. FT-IR testlerinde, katkısız ve asit katkılı membranların hepsinde karakteristik PBI değerleri gözlenmiştir ve ek olarak asit katkılı membranlarda, asidin etki ettiği alanlar açıkça görülmektedir. 4000-2000 cm^{-1} arasındaki tepe noktası, N-H uzaması ve 1000-1700 cm^{-1} arasındaki tepe noktası ise benzen/imidazol halkalarına aittir. 1620, 1530, 1440, 1280 ve 790 cm^{-1} değerlerindeki tepe noktaları, sırası ile güçlü C=C/C=N uzaması, 2-yer değiştirmesi karakteristiği, benzimidazolün düzlemdeki titreşim karakteristiği, C-N uzaması ve C-H eğilmesidir. 2920 cm^{-1} civarındaki tepe noktası ise N-H grubunu göstermektedir. C-N, H-N ve çember deformasyonları 2000-1000 cm^{-1} arasındadır. Membranlarda fosforik asit katkılaması, hidrojen bağları ve fosfat gruplarındaki hidrojenlerin titreşimi sebebi ile bazı tepe noktalarının görünürlüğünü önemli ölçüde azaltmıştır. Asit katkılaması 1495 cm^{-1} değerinde yeni tepe noktası oluşturmuştur ve bu da $C=NH^{+}$ grubundaki C=N titreşimleridir ve sebebi ise imino azot atomlarının protonlarıdır. 2500-3000 cm^{-1} aralığındaki geniş bant ise imid içindeki azot atomların protonlanmasından kaynaklanır ve fosforik asitten imidazol grubuna proton aktarımının sonucudur. Kompozit membranlarda, ÇDKNT ve PBI arasındaki kovalent olmayan π-π etkileşimleri sebebiyle ÇDKNTlerin değerleri seçilememektedir.

Tarayıcı elektron mikroskopisinde ise çok duvarlı karbon nanotüplerin dağılımı görülebilmektedir. Çok duvarlı karbon nanotüplerin uçlarının beyaz noktalar halinde görülmesi, birbirlerinden ayrı olması ve birikme olmaması, dağılımın homojenliğini göstermektedir.

Asit katkılı membranların protonik iletkenlikleri, elektrokimyasal empedans spektroskopisi yöntemiyle belirlenmiştir. İletkenlik testleri nemsiz ortamda gerçekleştirilmiştir. Empedans testlerinden elde edilen sonuçlar ile iletkenlikler hesaplanmıştır. 120 °C, 140 °C ve 160 °C sıcaklıklar için saf PBI membranın protonik iletkenliği sırasıyla 0.0518 S/cm, 0.0667 S/cm ve 0.0895 S/cm olarak hesaplanmıştır. Ağırlıkça %0.5 PBI/CDKNT membran için bu değerler 120 °C, 140 °C ve 160 °C için sırasıyla 0.0401 S/cm, 0.0586 S/cm ve 0.0613 S/cm iken, ağırlıkça %1 PBI/CDKNT membranda biraz daha fazla ve sırasıyla 0.0429 S/cm, 0.0621 S/cm ve 0.0655 S/cm olarak hesaplanmıştır.

1. INTRODUCTION

1.1 Fuel Cells

Fuel cells are highly efficient electrochemical energy converters, which operate with zero or low emissions. By direct chemical reactions between hydrogen and air, they produce DC electricity. They use pure hydrogen as fuel (as well as methanol and hydrocarbons for some types of fuel cells) and ambient air as oxidiser. At the end of the reactions, they produce either pure water, or low emission in addition to pure water, as waste. The gasses are fed to the cell and the catalyst layer ionises them to prepare to the electrolyte surface reactions. The conventional methods, such as combustion engines and turbine systems, convert fuel into heat, then heat to mechanical energy and finally, mechanical energy to electricity. The efficiency decreases with every step. Because of the absence of the intermediate steps, efficiency of the fuel cells is drastically higher. Fuel cells can have an electrical efficiency as much as 70% and when they operate as a co-generation system to use their excess heat, which is caused by the exothermic reactions in the cell, the overall efficiency rate can go up to 90% [1].

Fuel cells have gained popularity over the years due to their absence of intermediate steps and moving parts, which lowers the possibility of problems and maintenance costs. Their small sizes, silent operation conditions and huge power capacity scales (from W to MW) also have an important role.

Fuel cells consist three major parts; bipolar plates, electrodes and an electrolyte. Bipolar plates act as the current collectors and they cover the cell. Between the bipolar plates, there are the anode and the cathode electrodes. The fuel and the air are ionised here for the upcoming electrochemical reactions. And finally, the electrolyte serves as an ion carrier for the reactions, which mostly occur at the electrolyte surface.

Since their discovery in 1839 by British scientist William R. Groove as “gaseous voltaic cells”, many other fuel cell types were developed [2]. But the most important role in popularising the fuel cells belong to National Aeronautics and Space

Administration (NASA). While they were looking for a safe and efficient way to generate electricity for their spacecrafts in 1960s, they started to use alkaline fuel cells for their Apollo programme [3]. Today we can see fuel cells all around, from car engines (Mercedes-Benz GLC F-Cell, Toyota Mirai, Honda Clarity Fuel Cell, and Hyundai Nexo) to huge scale power plants (Daesan Industrial Complex, 50 MW, Hanwha Energy, Seosan, South Korea).

1.2 Types of Fuel Cells

Fuel cells are usually named after their electrolytes. There are mainly five types of fuel cells; alkaline fuel cells (AFCs), phosphoric acid fuel cells (PAFCs), molten carbonate fuel cells (MCFCs), solid oxide fuel cells (SOFCs) and polymer electrolyte membrane (or proton exchange membrane) fuel cells (PEMFCs). Sometimes direct methanol fuel cells can be regarded as a different type of fuel cells. However, because they use the same structure and materials as the PEMFCs, they are considered to be a part of that group.

Alkaline fuel cells use KOH/water solution as an electrolyte and OH^- ions are carried from the cathode to the anode side. Their operating temperature can vary between 30-250 °C. They can use valuable catalysts (noble metals) as well as Ni, Ag or metal oxides, depending on the temperature. They are intolerant to carbon poisoning. Their efficiency rate reaches up to 60% [2]. Their reaction occurs as stated in the equations (1.1) and (1.2) for the anode and the cathode layer, respectively.

$$H_2 + 2\,OH^- \rightarrow 2\,H_2O + 2\,e^- \tag{1.1}$$

$$^1/_2\,O_2 + H_2O\ +\ 2\,e^- \rightarrow 2\,OH^- \tag{1.2}$$

Phosphoric acid fuel cells use concentrated acid (~100%), kept in usually SiC matrix, as their electrolyte. Their catalyst is platinum (Pt). Operating temperature changes between 150- 220 °C. Because of their liquid electrolyte, they are suitable only for stationary application and are commercially available for this purpose. Their electrical efficiency is around 40-45% [2]. Their reaction follows the given equations in (1.3) and (1.4) for the anode and the cathode layer, respectively.

$$H_2 \rightarrow 2\,H^+ + 2\,e^- \tag{1.3}$$

$$^1/_2\,O_2 + 2\,H^+\ +\ 2\,e^- \rightarrow 2\,H_2O \tag{1.4}$$

Molten carbonate fuel cells use a molten carbonate salt mixture of alkali metals as the electrolyte. Their operation temperature is around 600-700 °C. They do not require expensive catalysts because of the high operating temperatures. Their electrical efficiencies are around 45-60% [2]. Their equations occur according to the following equations in (1.5) and (1.6) for the anode and the cathode layer, respectively.

$$H_2 + {CO_3}^{-2} \rightarrow H_2O + CO_2 + 2\,e^- \tag{1.5}$$

$$^1/_2\,O_2 + CO_2 \rightarrow 2\,e^- + {CO_3}^{-2} \tag{1.6}$$

Solid oxide fuel cells use a solid ceramic as the electrolyte. Their operating temperature ranges between 600-1000 °C, but their optimal working temperature is 800 °C. They have the highest electrical efficiency among the fuel cells with a rate of 70% [1]. When co-operated with a combined heat-power system, their overall efficiency can reach up to 90%, because of the use of their waste heat. Given their high operating temperatures, they do not require expensive catalysts such as Pt, and use Ni instead. They have the fuel flexibility because of the high temperature and can use humid carbon monoxide (CO) and hydrocarbons such as methane (CH_4) as fuel, as well as pure hydrogen. Because of their high operating temperature, they are best suited for stationary applications, such as power plants. However, there are some exemplary vehicles (such as busses), too. They generate electricity by following the equations in (1.7) and (1.8) for the anode and the cathode layer, respectively.

$$H_2 + O^{-2} \rightarrow H_2O + 2\,e^- \tag{1.7}$$

$$^1/_2\,O_2 + 2\,e^- \rightarrow + O^{-2} \tag{1.8}$$

Polymer electrolyte membrane (or proton exchange membrane) fuel cells are the most commonly used and commercialised fuel cells. Their electrical efficiency can reach up to 50% [2]. They use Pt or its composites as catalyst. Carbon supports, such as graphene oxide or carbon nanotubes, can be used to lower the Pt amount in order to reduce the price. Their operating temperatures are between room temperature to 120 °C for perfluoro-sulfonylfluoride ethyl-propyl-vinyl ether (Nafion) membranes and between 120-190 °C for polybenzimidazole (PBI) membranes. Both of these membranes are intolerant to carbon poisoning, so the carbon compounds in the gasses must be in ppm levels at most. Reactions in PEMFCs are the same as the reactions in PAFCs, given in equations (1.3) and (1.4).

1.3 Aim of the Study

The climate change advances faster than ever, and the need for the new ways to produce energy gains crucial importance every single day. Fuel cells have gathered attention in the last couple of decades as a replacement for the conventional energy sources along with solar and wind energy. Because of their high efficiencies combined with no (or low) emission, they are promising candidates for the future.

Among all the fuel cell types, PEMFCs are the most commonly used ones because of their quick start-up capability, as well as their accessibility. There are many car manufacturers, which commercially released fuel cell cars. There are also encouragements in certain places to buy and use these cars. In the year 2021, the state of California gives $15,000 worth of free hydrogen (worth of 67,000 miles, ~107,826.048 km) to those who own a Toyota Mirai [4]. However, there are drawbacks of PEMFCs, as well. Today, heat and water management come in the first place among these problems. In order to get rid of these problems, polybenzimidazole (PBI) membranes were introduced.

PBI is an alternative to Nafion; and unlike Nafion membranes, PBI membranes can operate at higher temperatures as much as 200 °C. In these high temperatures, heat and water managements are not a problem. They can also operate without humidification, so the costs decrease compared to Nafion membranes. The ionic conductivity of the PBI membranes increase with the increasing phosphoric acid doping level; however, higher levels of acid doping (more than 6 mol PA/PBI) can damage the membrane and decrease the mechanical strength. In order to overcome this problem, high molecular weight membranes are synthesised and used. In recent years, graphene or carbon nanotubes are also applied to this process because of their high mechanical strengths. Another advantage of this application is, that it lowers the gas permeability.

In this study, we firstly synthesised and characterised PBI polymer. Then we added multi-wall carbon nanotubes (MWCNTs) to the PBI solutions to increase the protonic conductivity. The film casting method was used to obtain the membranes. After that, the PBI membranes were doped with 85wt% phosphoric acid (H_3PO_4). Finally, we characterized the polymer and the membranes by Nuclear Magnetic Resonance Spectroscopy (NMR), Scanning Electron Microscopy (SEM), X-Ray Diffraction

(XRD), Fourier Transform Infrared Spectroscopy (FT-IR), Thermogravimetric Analysis (TGA) and Electrochemical Impedance Spectroscopy (EIS).

2. LITERATURE

PEMFCs are made of bipolar plates, gas flow channels, gas diffusion layers, catalyst layers and a membrane. The operating principles of PEMFCs are given in Figure 2.1. The electrochemical reactions take place in the catalyst layers and intensify closer to the electrolyte surface. Hydrogen ionises in the anode side through the catalyst layer and the H^+ ions go through the membrane to the cathode side. These positive ions meet with O^{-2} in the cathode side and they produce pure water as waste [5,6]. The electrons go through the external circuit, which connects the bipolar plates, and generate electricity.

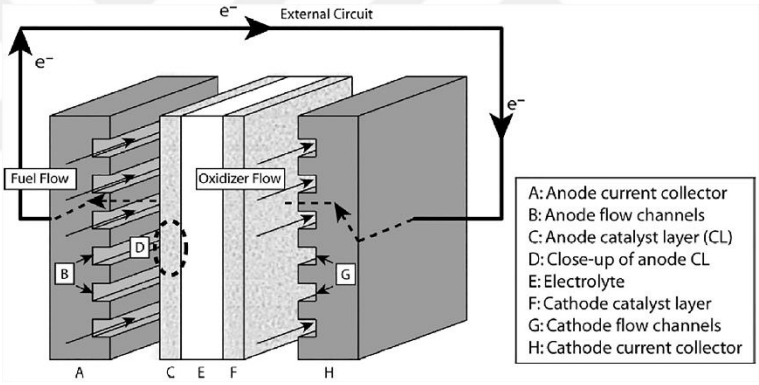

Figure 2.1: Operating principles of a PEMFC [6].

While PEMFCs work, their membranes constantly absorb water from the humid gasses due to electro osmotic forces; thus, they swell and their dimensions change. This dimension change must be taken into consideration while designing a PEMFC [2,3,5].

Nafion is the most commonly used PEMFC membrane, and their optimal operating temperature is around 80 °C [3]. Humidity is very important for Nafion membranes, because their conductivity increases with the humidity. Under normal conditions around 120 °C, these membranes can no longer be used, however, it is possible to operate with Nafion at this temperature with high pressure and humidity. Higher temperatures are preferred to overcome the issues, such as water condensation, heat management and impurity tolerance. Nevertheless, these applications are complex and increase the costs. As an alternative to Nafion membranes, PBI membranes were

introduced in 1995 [7]. PBI membranes operate at higher temperatures, around 160-200 °C. At these temperatures, mentioned problems, such as water condensation and impurity tolerance are no longer problems and useful heat can also be recovered. With the studies made throughout the years, it was seen that PBI has good thermal balance and low gas permeability compared to Nafion [8,9].

PBI membranes have their own problems, too. Pristine PBI membranes are not good proton conductors. Thus, they have to be doped with phosphoric acid. It is crucial to dope the membrane to achieve usable conduction levels. However, this doping decreases the mechanical strength of the membrane. There are studies focusing on this problem [10,11]. In these studies, they aim to keep the good conduction level while lowering the acid doping in the long-term use. Gas permeability is also a problem no matter how dense the membrane is, because hydrogen is the smallest element and it leaks easily. In order to eliminate this problem, support materials are added to the membrane [12,13].

2.1 Thermodynamic and Electrochemical Investigation of PEMFCs

A PEMFC operates at room temperature according to following reactions in (2.1), (2.2) and (2.3) as the anode layer reaction, the cathode layer reaction and the total reaction, respectively.

$$H_2 \rightarrow 2\,H^+ + 2\,e^- \tag{2.1}$$

$$^1/_2\,O_2 + 2\,H^+ + 2\,e^- \rightarrow 2\,H_2O \tag{2.2}$$

$$H_2 + {}^1/_2\,O_2 \rightarrow H_2O \tag{2.3}$$

$$\Delta H = -286\ kJ/mol$$

ΔH is the enthalpy of the reaction. The electrical energy that can be converted into a useful (electrical) energy is the Gibbs free energy (ΔG) of the cell. Entropy (ΔS) causes some irreversible energy losses. Gibbs free energy equation is given in (2.4).

$$\Delta G = \Delta H - T.\Delta S \tag{2.4}$$

The generated electricity of a cell is;

$$W_{el} = q.E \tag{2.5}$$

In this equation, W_{el} is electrical work (Joules/mol), q is charge (coulombs/mol) and E is potential (Volts). The sum of the charges transferred in membrane divided by one mol of hydrogen gas is;

$$q = n.N_{Avg}.q_{el} \tag{2.6}$$

where n is the number of electrons per H_2 molecules (2 electrons/molecule), N_{Avg} is the Avogadro's number ($6.022\,x\,10^{23}$ molecules/mol), q_{el} is the charge of one electron ($1.602\,x\,10^{-19}$ coulombs/electron). N_{Avg} and q_{el} together yield the Faraday's constant F (96,485 coulombs/electron-mol). Thus, electrical work becomes;

$$W_{el} = n.F.E \tag{2.7}$$

It was stated earlier that the Gibbs free energy gives the electrical work of a cell;

$$W_{el} = -\Delta G \tag{2.8}$$

Thus, the theoretical potential of a cell becomes;

$$E = {}^{-\Delta G}/_{n.F} \tag{2.9}$$

ΔG can be calculated by using the thermodynamical tables, n and F are constants, given above. This means, that the theoretical value of a hydrogen/oxygen fuel cell at 25 °C is;

$$E = 1.23\,Volts$$

The effect of different temperatures is given in Table 2.1.

Table 2.1: The effect of different temperatures on a PEMFC [3].

T (°C)	E (Volts)
25	1.230
60	1.200
80	1.184
100	1.167

The pressure also plays an important role on the operation of fuel cells. A fuel cell can operate in pressures from atmospheric to 6-7 bar. For an isothermal process, the change in Gibbs free energy can be written as;

$$dG = V_m.dP \tag{2.10}$$

In this equation, V_m is molar volume (m^3/mol) and P is pressure (bar). If we use the equation (2.10) in the ideal gas equation;

$$dG = RT.{}^{dP}/_{P} \tag{2.11}$$

And after the integration;

$$G = G_0 + RT.\ln\left({}^{P}/_{P_0}\right) \tag{2.12}$$

where G_0 is the Gibbs free energy at standard conditions and the P_0 is the reference condition (1 atm).

For a chemical reaction given as below;

$$jA + kB \rightarrow mC + nD \tag{2.13}$$

the change in Gibbs free energy is;

$$\Delta G = mG_C + nG_D - jG_A - kG_B \tag{2.14}$$

When we write equation (2.14) into the equation (2.12);

$$\Delta G = \Delta G_0 + RT\ln\left[\frac{\left(\frac{P_C}{P_0}\right)^m\left(\frac{P_D}{P_0}\right)^n}{\left(\frac{P_A}{P_0}\right)^j\left(\frac{P_B}{P_0}\right)^k}\right] \tag{2.15}$$

This equation is the Nernst Equation. P is the partial pressure of the gas. For a PEMFC reaction, it is written as;

$$\Delta G = \Delta G_0 + RT\ln\left[\frac{P_{H_2O}}{P_{H_2}P_{O_2}^{0.5}}\right] \tag{2.16}$$

When the equation (2.17) is written in the equation (2.16), it gives the equation (2.18).

$$E = -\left(\frac{\Delta H}{nF} - \frac{T\Delta S}{nF}\right) \tag{2.17}$$

$$E = E_0 + \frac{RT}{nF}\ln\left(\frac{P_{H_2}P_{O_2}^{0.5}}{P_{H_2O}}\right) \tag{2.18}$$

With this equation, only the potential of the gaseous reaction can be calculated. In case of introduction of liquid water, partial pressure of the water in the equation becomes 1.

There are mainly 3 types of losses in fuel cells; activation polarisation, ohmic (resistive) polarisation and concentration polarisation. The loss mechanism can be expressed as;

$$E_{cell} = V_{OC} - E_{polarisation} \tag{2.19}$$

E_{cell} is the maximum voltage, that the cell can yield. V_{OC} is the open circuit voltage (OCV) of the cell, which is the real maximum amount of voltage. When we write the mentioned polarisation losses into $E_{polarisation}$,

$$E_{cell} = V_{OC} - E_{activation} - E_{ohmic} - E_{concentration} \tag{2.20}$$

There is a certain amount of energy required to start the chemical reactions. This is called the activation energy, which causes the activation polarisation and its reason is the slow electrode kinetics. This loss decreases with the increasing exchange current density. Activation polarisation occurs both in the anode and the cathode, however, it is much higher in the cathode due to the higher activation overpotential of the oxygen reduction reactions. $E_{activation}$ can be written according to Butler-Volmer Equation,

$$E_{activation} = \frac{RT}{\alpha F} \ln\left(\frac{i}{i_0}\right) \tag{2.21}$$

In this equation, R is the gas constant, T is the temperature (K), α is the transfer coefficient, i is the current density (A/cm^2) and i_0 is the exchange current density (A/cm^2). The exchange current density dictates the equality of the surface concentration to bulk concentration. In case of hydrogen crossover in the membrane or internal current loss, these values are not equal to one another. i_0 is expressed as,

$$i_0 = i_{0,ref} a_c L_c \left(\frac{P_r}{P_{r,ref}}\right)^{\gamma} exp\left[-\frac{E_C}{RT}\left(1 - \frac{T}{T_{ref}}\right)\right] \tag{2.22}$$

Here, a_c is the catalyst specific area, L_c is the catalyst loading, P_r is the reactant partial pressure, γ is the pressure coefficient (0.5-1.0) and E_C is the activation energy required for O_2 reduction on the catalyst.

Ohmic polarisation is caused by the flow of the ions through the electrolyte and electrons through the electrically conductive parts. Even though the electrical resistance is almost completely negligible, the resistance of the electrolyte is too high to neglect. E_{ohmic} can be written according to Ohm's law,

$$E_{ohmic} = iR_i \tag{2.23}$$

where R_i is the total internal resistance.

Concentration polarisation is caused by the fast consumption of the reactant gasses. In this case, concentration gradients occur, which causes partial pressures to drop in

equation (2.18). This results in a voltage drop. $E_{concentration}$ can be written according to the Nernst Equation,

$$E_{concentration} = \frac{RT}{nF}\ln\left(\frac{i_L}{i_L - i}\right) \tag{2.24}$$

When the equations (2.21), (2.23) and (2.24) are written in the equation (2.20), a scientifically accurate approximation of the cell voltage can be obtained and expressed as follows;

$$E_{cell} = V_{OC} - \frac{RT}{\alpha F}\ln\left(\frac{i}{i_0}\right) - iR_i - \frac{RT}{nF}\ln\left(\frac{i_L}{i_L - i}\right) \tag{2.25}$$

This equation results the polarization curve in Figure 2.2.

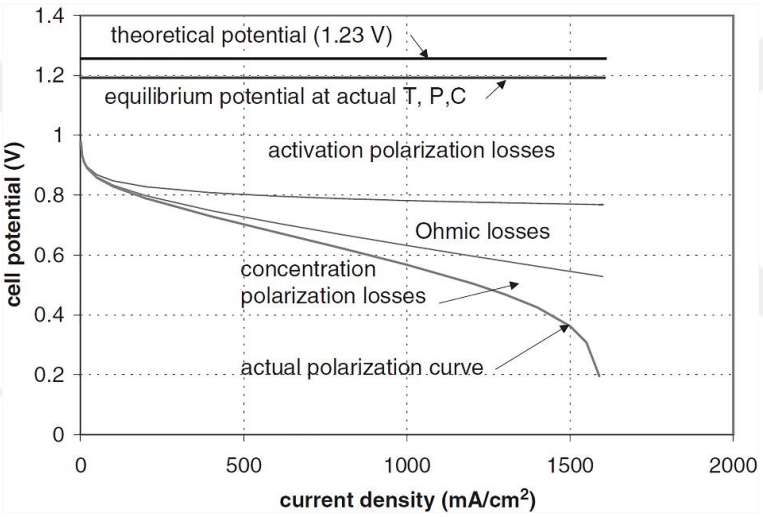

Figure 2.2: Polarization Curve of a PEMFC [3].

2.2 Electrical Efficiency of a PEMFC

The efficiency of an energy conversion device is calculated by dividing the useful energy output to the energy input. In the case of PEMFCs, the energy input is the enthalpy of hydrogen and the useful energy input is the electrical energy. Thus, the maximum theoretical efficiency of a PEMFC is;

$$\eta = {}^{\Delta G}/_{\Delta H} = {}^{237.34}/_{286.02} = 83\% \tag{2.26}$$

The enthalpy value here is the higher heating value of hydrogen. In many cases this is the form of calculating. However, compared to internal combustion engines, this is not the case; because in the combustion engines, lower heating value of the fuel is used in order to calculate the efficiency. This situation is explained by the production of the water vapour. Both values can be used to calculate the efficiency, as long as which one

used is stated. In case of using the lower heating value of hydrogen, the result changes as;

$$\eta = {}^{\Delta G}/_{\Delta H_{LHV}} = {}^{237.34}/_{241.98} = 94.5\% \quad (2.27)$$

Nevertheless, it is thermodynamically correct to use the higher heating value of the fuel because it considers all the available energy. In combustion engines, they do not take the heat of condensation of product water into consideration. However, the heat of condensation is actually used by the boilers. Thus, it is more consistent to use the higher heating value with the definition of efficiency.

2.3 Polybenzimidazole (PBI) Polymer and Membranes

PBI polymer is a linear heterocyclic polymer made of benzimidazole group. They are considered thermoplastics, since they have linear chains. PBI was first introduced in 1959 by Brinker et al. [14] as an aliphatic PBI. Then in 1960, Vogel et al. [15] introduced the fully aromatic PBI. PBIs, especially fully aromatic ones, have excellent thermal stability because of the intermolecular hydrogen bonds present in the structure; their decomposition starts above 400 °C. They also yield high toughness as well as stiffness, resistance to chemicals and stable phenyl groups [16]. The single benzimidazole group is given in Figure 2.3.

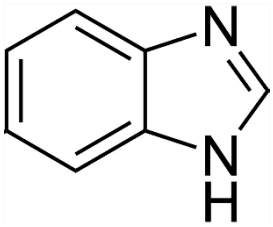

Figure 2.3: The single benzimidazole group [18].

There are many PBI polymer types, and poly [2,2'-(m-phenylene)-5,5'-bibenzimidazole] (m-PBI), given in Figure 2.4, is the most commonly used and commercially available one. Three phenyl groups attached to the repeating units give the polymer excellent properties. Decomposition of m-PBI starts around 430 °C and it does not have a melting point. TGA analysis in dry air yields a decomposition temperature between 450-500 °C [17].

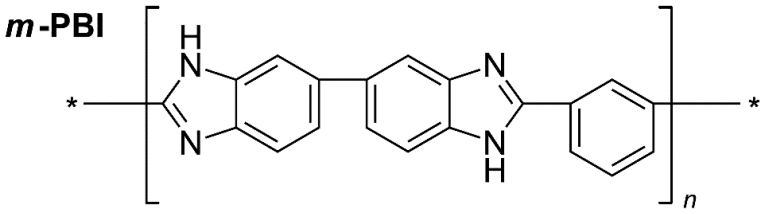

Figure 2.4: The m-PBI polymer [18].

PBI Performance Products, Inc. sells different types of PBI membranes under the name of Duratron (formerly known as Celazole), as well as Danish Power System's Dapozol. Throughout the years, deep researches on the subject were made because of its non-flammability, processability, thermal and chemical stabilities.

Because of its excellent properties, m-PBI has a wide range of application area. It is used as reverse osmosis membranes due to its high chemical stability as well as mechanical strength. It can be used as a sorption material for aqueous SO_2, separation tool for CO and acids. It is also used in space technology, such as astronaut clothes and spaceship wings. In higher temperatures and flaming conditions, it is used with acid doping (sulphuric or phosphoric acid), so that its dimensional stability can improve [19], which makes it suitable for firemen clothing. It is also used in catalyst layers as a support structure due to its high chemical stability [20-24]. As an electrical insulator material and moisture resistance, it is sought after for semiconductors and electrical circuits. Its low dielectric constant and low tangent loss, meaning low radar observability, makes it a suitable candidate for military applications.

2.3.1 m-PBI synthesis

Although there are many different synthesis procedures for m-PBI, two of the methods are dominantly common; melt/solid polycondensation [15] and solution polymerisation [17].

The solid polycondensation method contains an aromatic tetraamine called diaminobenzidine (DAB) and a carboxylic acid called diphenyl isophthalate as monomers. The monomers are put into an inert reactor purged with nitrogen. Then they are mixed throughout the process at 200 °C, the melting temperature. At this point, phenol change can be observed clearly. Continuous heating results in high viscosity and the reaction ends when the product solidifies. After that, the mixing stops and vacuum is applied to remove the water vapour and free phenol in the atmosphere. Then when the material is cooled down to the room temperature, it is pulverised and

put into the polymerisation tube. Heat is applied again under vacuum until the temperature reaches 350-400 °C. At this point, high molecular weight polymer is obtained. Figure 2.5 shows the reaction. In the solution polymerisation method, diaminobenzidine tetrahydrochloride hydrate (DAB.4HCl.xH_2O) is generally used, because it is less sensitive to oxidation. As a phenylene source, an aromatic carboxylic acid or its derivatives are used.

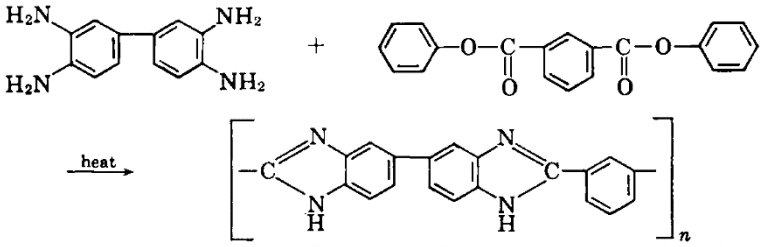

Figure 2.5: Solid/melt polycondensation [17].

Polyphosphoric acid (PPA) is used as a solvent and condensing agent. The solution polymerisation method is as follows: a certain amount of PPA is put into an inert reactor and heated to 140 °C. Then DAB.4HCl.xH_2O is added and mixed for two hours (or more if necessary) to eliminate all the HCl gas bubbles. Then the solution is heated to 170 °C and the carboxylic acid group is added. After some time, the reactor is heated to 200 °C and reaction takes place for around 20 hours. Meanwhile the solution becomes highly viscous. After the reaction ends, it is poured into DI water to isolate the polymer. Then it is washed thoroughly and dried. Figure 2.6 shows the reaction.

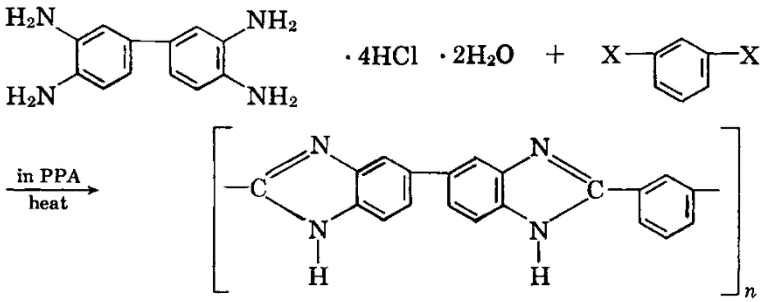

Figure 2.6: Solution polymerisation [17].

2.3.2 Phosphoric acid doping of PBI membranes

Phosphoric acid (H_3PO_4) doping is the most successful way to enhance the protonic conductivity of the PBI membranes. This high protonic conductivity as a result of acid doping is caused by the hydrogen bonds between hydrogen and imidazole rings in the PBI. As stated before, it was first used in PEMFCs in 1995 by Wainright et. al [7].

Since then, extensive researches were made and still are still being made on the subject [25-30]. Studies on the subject mostly focus on mechanical strength, ionic conductivity, gas permeability and fuel cell performance, as well as its non-humid operating temperatures.

PBI membrane can be obtained via sol-gel method by directly casting the viscous liquid after the reaction or simply by casting the PBI solution into a petri dish. In order to do this, PBI polymer must be dissolved in a solvent, such as N,N-dimethylacetamide (DMAc) with LiCl for a good solubility, for a certain amount of time. The solution should contain 5-20wt% PBI. Below 5wt%, polymer chains cannot form compact and complex structures to form a membrane. Above 20wt%, a homogenous solution cannot be obtained [31]. After that, it can be poured into a petri dish to obtain the membranes. Finally, the membranes are immersed in the phosphoric acid for doping. The doping can be carried out in a room temperature for several days or 30 minutes in 90 °C acid [32].

The conductivity of the membranes relies on acid doping level and temperature. The humidity is not crucial in PBI membranes as it is for Nafion membranes. There are two reasons for this; first one is that there is a denser acid medium which acts as a both hydrogen donor and acceptor, and the second reason is the drag coefficient of water is almost zero. However, in case of high humidity, the water content of the membranes increases. This results in a lower viscosity of the membrane; which increases the free ion movement and the protonic conductivity [7].

There are two proton conduction mechanisms in the acid doped membranes. One of them is the diffusion of protons through the free acid in the membrane. The other proton conduction mechanism is known as the Grotthuss mechanism. Grotthuss mechanism is the mechanism, which protons advance by hopping from one molecule to the other. There are some results that agree with this mechanism. The conductivity results are in good agreement with the Arrhenius' Law given in equation (2.28).

$$\sigma = A \exp\left(\frac{-E_a}{RT}\right) \tag{2.28}$$

A is the pre-exponential factor and E_a is the activation energy required for proton transfer. ${HPO_4}^{-2}$ and H_2PO^- anions help this hopping [33]. This hopping mechanism is presented in Figure 2.7.

The tensile strength of a pristine PBI membrane at room temperature is around 100-160 MPa [35-37]. However, after acid doping, this value decreases to ~13 MPa at room temperature, and ~2 MPa at 150 °C, and as the doping level rises, the tensile strength sinks [8].

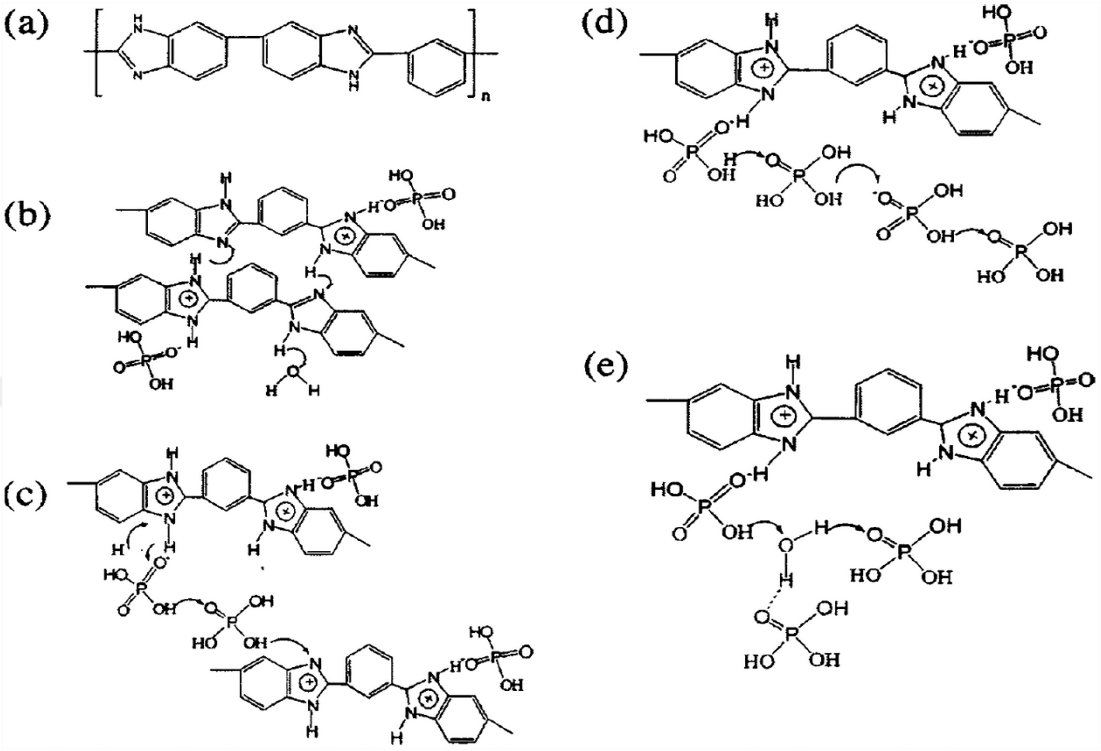

Figure 2.7: The Grotthuss mechanism. (a) Structure of PBI, (b) H_3PO_4 doped PBI, (c) proton transfer along acid-BI-acid, (d) proton transfer along acid-acid, (e) proton transfer along acid-H_2O [34].

2.3.3 Carbon nanotube supported PBI membranes

Carbon based support materials are no strangers to fuel cells. Especially graphene oxide (GO), carbon nanotubes (CNT) and carbon black (CB) are widely used in catalysts in order to lower the platin (Pt) amount, while maintaining the high electrical conductivity. Although these materials have good electrical properties, they are used in electrolytes, as well. The main reason of utilization in electrolytes is, however, not to enhance the electrical conductivities, but to increase the mechanical strength and protonic conductivity, while trying to decrease the gas permeability [38-46]. Graphene oxide (GO) is usually sprayed onto the PBI membrane, dried, and another layer of PBI is sprayed on it, in order to achieve a sandwich structure and trap the GO layer inside the PBI, so that the electrical conductivity of GO is eliminated. GO can be added to the PBI solution also.

When it comes to carbon nanotubes, multi-walled carbon nanotubes (MWCNTs) are used in the membranes. They are added to the PBI/DMAc solution before preparing the membranes, contrary to spray method of GO. The amount of MWCNTs should not exceed the 1% of the PBI polymer, otherwise the membrane will become electrically conductive.

Guerrero Moreno et al. [47] prepared 1% non-functionalised MWCNT added PA doped PBI (PBI-CNT) composite membranes for HT-PEMFCs and compared it to the pristine PBI membranes. PBI-CNT membranes had higher protonic conductivity of 0.074 S/cm and OCV of 0.96 V while PBI membranes had protonic conductivity of 0.063 S/cm and OCV of 0.8 V. Composite membranes also yielded higher tensile strength with a rate of 32%.

Wu et al. [48] prepared KOH doped MWCNT-PBI membranes with different ratios (0.05%, 0.1%, 0.15% and 1% functionalised MWCNTs) for direct methanol fuel cells. They observed that the methanol permeability decreased from 2.59×10^{-10} m^2/s to 1.85×10^{-10} m^2/s, while the protonic conductivity increased from 0.023 S/cm to 0.035 S/cm, with respect to the increasing MWCNT amount.

Suryani et al [49] prepared different membranes with MWCNTs. Their composite membranes had 0.085 S/cm, while the pristine PBI membranes had 0.045 S/cm protonic conductivity. Moreover, their pristine PBI membranes had 54 MPa of tensile strength and composite MWCNT-PBI membranes had 80-100 MPa.

Kannan et al. [50] achieved an increase in the tensile strength with functionalised MWCNTs in their membranes from 65 MPa (pristine PBI) to 100 MPa (MWCNT-PBI). They also observed an increase in the protonic conductivity from 0.073 S/cm to 0.120 S/cm.

Shao et al. [51] proposed a new “one pot” method to synthesise PBI and add sulfonated MWCNTs in it. They measured the tensile strength of pristine PBI as 99 MPa and 138 MPa for the MWCNT/PBI.

Jheng et al. [32] obtained PBI membranes with different functionalised MWCNTs. They measured the tensile strength as 42.5 MPa for pure PBI membrane and 57.4 MPa for 0.3wt% MWCNT/PBI membrane. They also measured an increase in the protonic conductivity from 0.0056 S/cm (pristine PBI) to 0.0066 S/cm (MWCNT/PBI).

2.4 Characterisation Methods

2.4.1 Physical characterisation techniques

2.4.1.1 Nuclear magnetic resonance (NMR) spectroscopy

1H-NMR test gives the proton resonances in the compound, which enables one to determine the bonds and molecules within the sample. The sample is first dissolved in a deuterated solvent. The amount of the dissolved sample will determine the intensity of the peaks later in the graphic. When the sample is placed into the NMR machine, the nuclei of some atoms will act like magnets in the strong magnetic field. This is due to the specific resonance level of the atoms. This way, the resonances are measured and turned into a graphic to analyse the sample, which contains peaks. After correcting the signal by phase shifting and base line correction in the NMR reading software, the peak values can be read. Each hydrogen atom resonates in a specific range, according to the bonds they make and compounds, to which they belong. By reading these values, the molecular structure of the sample can be obtained. Small impurity peaks, as well as water and solvent peaks are also visible in the graphic and they should be discarded.

2.4.1.2 Thermogravimetric analysis (TGA)

TGA analyses are used to measure the thermal stability of the materials. The sample is placed into the machine, onto a very sensitive scale. Then it is heated up in a constant manner in a gas environment (could be an inert or a reactive gas) and the weight drop is measured. In this procedure, the destruction temperature of the material can be recorded, which gives the thermal characteristic of the material.

2.4.1.3 X-Ray diffraction (XRD)

XRD analyses are used to determine the crystallographic structure of the materials. XRD machine irradiates X-rays onto the sample and measures the intensities, as well as scattering angles of the X-rays. Then it compiles the results to give a graphic about the crystalline structure. However, the samples can be partially crystalline (which means a periodical structure order, such as a polymer) or non-crystalline, too.

2.4.1.4 Fourier transform infrared (FT-IR) spectroscopy

FTIR analyses are used to determine the organic and functional groups in materials by measuring the wavelength ranges in the infrared zone, which are absorbed by the

material, to identify the chemical bonds. Then the machine compiles these results to yield a graphic and the bonds can be identified using the peaks in the graphic. Thus, the chemical structure can be ensured along with other tests, such as NMR, XRD, TGA, etc.

2.4.1.5 Scanning electron microscopy (SEM)

SEM works by scanning electrons on a sample in a vacuum chamber to get a magnified image. The samples must be electrically conductive, and if not, they must be coated with a conductor material beforehand. SEM are great tools to characterise the materials, which cannot be clearly seen through an optical microscope, such as nano structures. By doing so, these structures (or their dispersion in a material) can be characterised.

2.4.1.6 The tension tests

These tests are applied to gather the data on the mechanical strengths of the materials and their identifying values, such as modulus of elasticity, strain and yield strength. A constant pulling force is applied to record the sample's response. With this information, material can be mechanically characterised and applied to necessary areas or can be improved. Combined with FT-IR or NMR results, the comments on the reasons of the strength can be made.

2.4.2 Electrochemical characterisation techniques

2.4.2.1 Electrochemical impedance spectroscopy (EIS)

Electrochemical reactions occur as a result of the electron transfer in the cells. These reactions consist mostly the following; electrolyte resistance, charge transfer, mass transfer and finally, adsorption of electroactive species [52]. Electrical circuits are used to represent these processes. Randles-Ershler circuit model is the most popular one due to its content of electrolyte, mass transfer and charge transfer resistances, as well as double-layer capacitance.

In order to successfully analyse each component in the cell, as well as the electrochemical reactions, AC impedance spectroscopy is widely used. A small AC current is used with a DC current in an interval of frequency. By doing so, the impedance change is measured. In the OCV of fuel cells, the anode (due to fast anodic

kinetics) and the mass transfer can be neglected. A representation of a typical Nyquist plot of both low and high frequency regions is given in the Figure 2.8. However, they cannot always be so clearly seen. The relationship between the charge transfer resistance (R_{ct}, lower frequencies) and the Warbung impedance (Z_w, higher frequencies) yields the shape of the curve. In case of slow kinetics, charge transfer resistance will be high, which may result in an unobtrusive mass transfer region in the plot. In the contrary case, the charge transfer resistance will be so small, so that the mass transfer shall have a huge impact on the plot and the semicircular region may not be visible at all. This is due to the fractional amount of charge transfer resistance in comparison to ohmic resistance and the Warbung impedance.

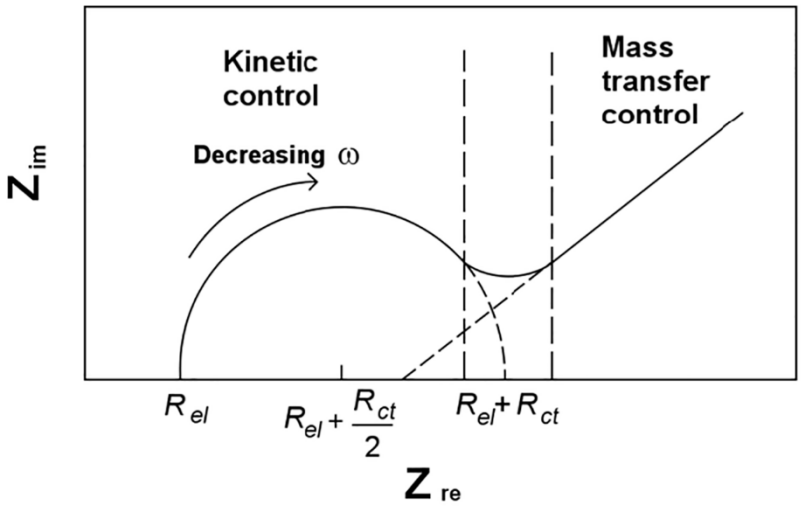

Figure 2.8: Impedance plots of real electrochemical systems in the complex plane [52].

Lower frequencies should be inspected in order to obtain the total resistance of the electrolyte and charge transfer resistance. The total impedance of a fuel cell electrical circuit (Z(ω)) is given in Figure 2.9.

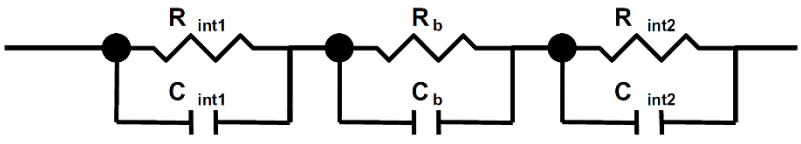

Figure 2.9: Electrical circuit of a fuel cell [53].

In this ideal circuit, R_{int} and C_{int} are the impedances between the membrane and the electrodes, R_{bulk} and C_{bulk} are the bulk membrane resistance and capacitance, respectively.

For impedance measurements of membranes in PEMFCs, four-probe and two-probe impedance methods are widely used. In the four-probe method, the membrane is placed between the four probes, the voltage and the current probes are on each side, and the current runs through the outer probes while measuring the voltage through inner probes. In the two-probe method, voltage and current electrodes are shorted. Thus, the Nyquist and Bode plots are obtained by the impedance analysis in a specified frequency range. From these plots, the resistance of the membrane (R_m), which occurs at high frequencies, is calculated by finding the zero point at the imaginary part in the plot. After that, using the equation (2.29) the protonic conductivity (σ) is calculated.

$$\sigma = \frac{D}{w_m . t_m . R_m} \tag{2.29}$$

where w_m is the width of the membrane and t_m is the thickness of the membrane. D is the distance between the voltage measuring inner probes in the case of in-plane measurements, whereas it is the thickness of the membrane in the through-plane measurements.

The results depend greatly on the distance between the probes [52]. Whether it is four-probe or two-probe, the reliability of the measurements increases with the increasing distance. Although it is considered that the four-probe method gives more accurate results, two-probe method also yields reliable data [52]. In order to achieve reliable results, it is enough to increase the frequency range [54].

2.4.2.2 Cyclic voltammetry (CV)

Cyclic voltammetry is a useful tool to obtain knowledge about the electrochemical reactions occurring within the cell. Three-probe measuring system is used in CV tests. In this method, the voltage of the working electrode is scanned between a set of values, then reversed. The electrochemical response of the species can be gathered in the process. Figure 2.10 shows an example on this data. While potential of the cell changes between these values, a cyclic voltammogram graphic is obtained.

The response of the current mainly depends on the analyte, analyte diffusion coefficient, scan rate, reaction rate, electrolyte type and finally, working electrode material. It is important that the working electrode is made of an inert material, such as platin or gold. Figure 2.11 shows a typical cyclic voltammogram of a reversible process.

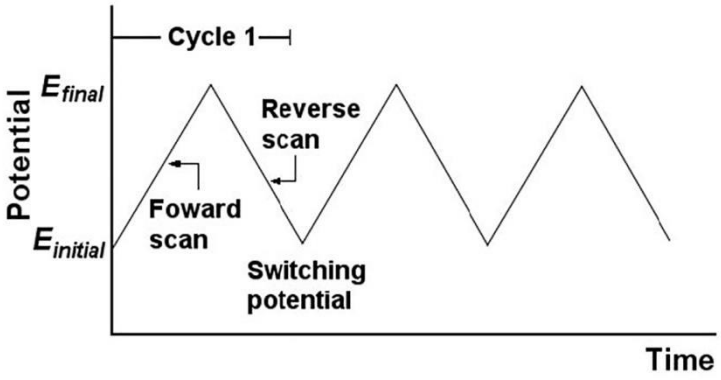

Figure 2.10: Voltage – time relation of CV signals [52].

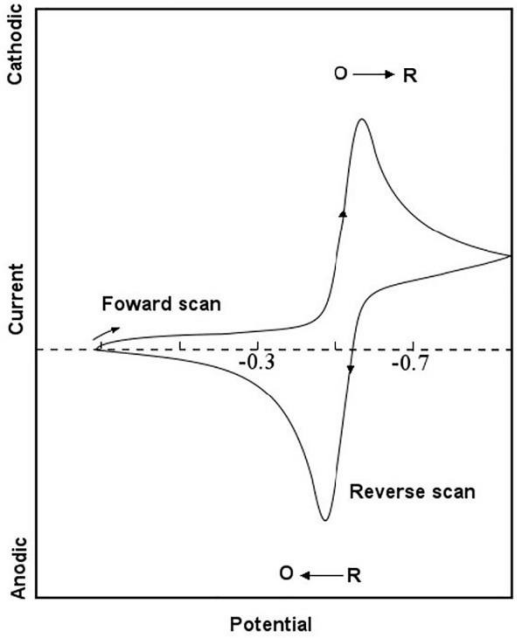

Figure 2.11: Typical cyclic voltammogram of a reversible process [52].

In the forward scan, reduction of oxidized form (O) begins and the voltage goes forward. The peak is limited by the mass transfer rate of O. The decrease in the curve is resulted by the expansion of the diffusion layer close to electrolyte. In the reverse scan, the result of the forward scan, which is called reduced species (R), is oxidised back to O.

3. EXPERIMENTAL

3.1 Materials

3,3′-Diaminobenzidine tetrahydrochloride hydrate (DAB.4HCl.xH_2O, ≥96%, Sigma-Aldrich) and isophthalic acid (IPA, 99%, Sigma-Aldrich) were used as the monomers; and polyphosphoric acid (PPA, reagent grade 115%, Sigma-Aldrich) was used as the polymerisation agent. During the reaction, pure nitrogen gas was used to make the atmosphere inert and calcium chloride (technical grade) was used in a drying tube. After the reaction, sodium bicarbonate (ACS reagent, ≥99.7%, Sigma-Aldrich) and methanol (anhydrous, 99.8%, Sigma-Aldrich) was used to wash and filter the polymer. For solution casting, N,N-Dimethylacetamide (DMAc, ReagentPlus®, ≥99%, Sigma-Aldrich) was used. Acid doping of the membranes were conducted via o-phosphoric acid (PA, 85%, Sigma-Aldrich). Multi-walled carbon nanotubes (MWCNTs) were synthesised in Istanbul Technical University, Energy Institute, Material Production and Preparation Laboratory, by using the chemical vapour deposition method at 500 °C, using acetylene.

3.2 Synthesis

Solution polymerisation method was used to synthesise the PBI polymer. A three necked round-bottom glass flask was connected to the nitrogen tube in one neck and a U-shaped drying tube filled with $CaCl_2$ in the other. From the top neck, a mechanical stirrer was placed into the flask. Then the flask was put in a vegetable (sunflower) oil bath. The temperature controller was placed in the oil. 60 gr of PPA was put into the flask and heated to 140 °C and dried for 3 hours in the nitrogen atmosphere. Then 6.28 mmol (2.2641 gr, 1/26.5 of PPA) of DAB.4HCl (dried in the oven overnight at 120 °C, so the xH_2O part is out of the material) was added slowly under a thin stream of nitrogen and left to be stirred for 2 hours in order to completely eliminate the HCl gas bubbles. After 2 hours, the temperature was raised to 170 °C, mixing speed was decreased and 6.28 mmol (1.0445 gr) of IPA (equimolar with DAB) was added to the

solution. The temperature was raised to 200 °C after 4.5 hours and kept there for 24 hours. The solution became viscous as the reaction progressed. The experimental setup is given in Figure 3.1.

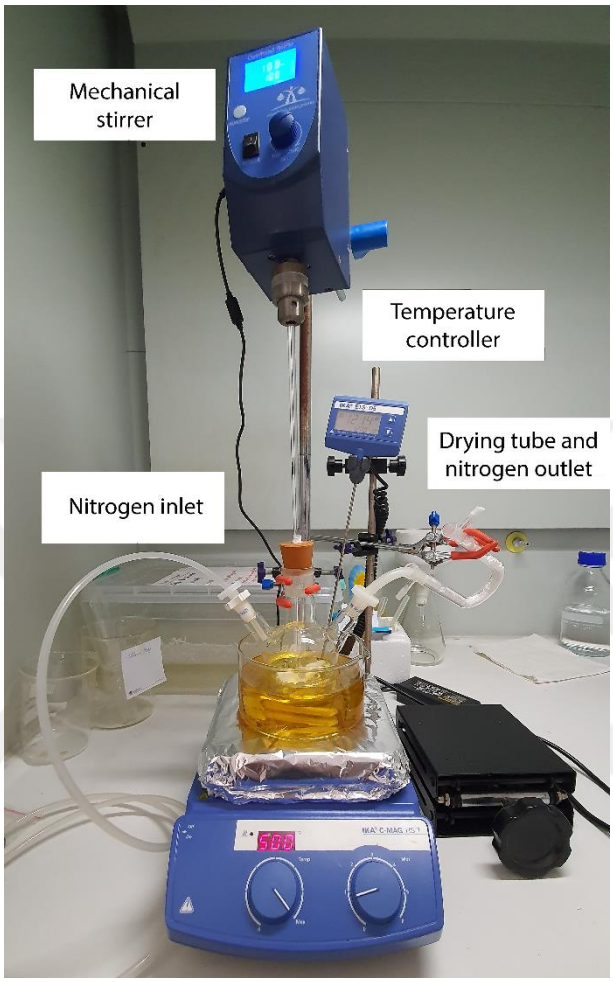

Figure 3.1: The experimental setup.

The polymerisation reaction occurs as given in Figure 3.2.

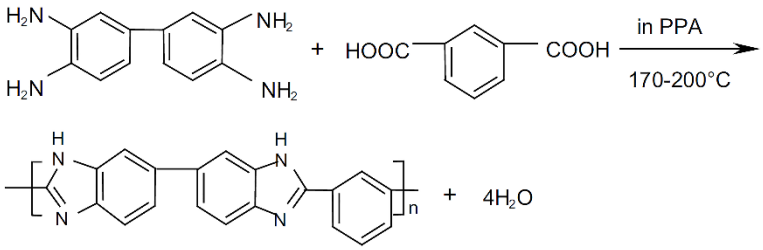

Figure 3.2: Polymerisation reaction of PBI.

After the reaction was completed, the viscous solution was poured into a beaker filled with room temperature DI water to initiate the polymer isolation process. The solution precipitated as soon as it met with the DI water, and became a PBI fibre. After that,

the polymer isolated with vacuum filtering. Then, it was washed with plenty of DI water and filtered again (pH = 2). After the filtering, the precipitate was put into a 5wt% sodium bicarbonate ($NaHCO_3$) solution and kept overnight while still being stirred, to increase the pH to a neutral state. Figure 3.3 shows the PBI fibre.

Figure 3.3: The PBI fibre.

The next day, the solution was filtered again (pH = 7.5) and washed with plenty of DI water and then some methanol (pH = 8.5). Finally, the solid polymer was dried in the oven at 150 °C overnight, grounded and stored in a desiccator. Figure 3.4 shows the dry product.

Figure 3.4: The final dry PBI product.

3.3 Membrane Preparation

The membranes were fabricated by solution casting method. 3wt% DMAc/LiCl solution was firstly prepared. The membrane thicknesses were calculated by using the density of the polymer and the volume of the desired membrane (based on the diameter of the petri dish). By doing so, the weight of the required polymer was calculated. After that, 5wt% PBI powder was added to the solution and stirred magnetically at 80 °C for two hours. Then it was centrifuged to eliminate the impurities, but because of the complete solution of the polymer, there was no aggregation. Then the solution was cast into a petri dish and put in the oven at 80 °C overnight. To peel off the membranes, warm DI water was poured into the petri dish, and after a couple of minutes, the membranes were easily peeled. Then they were put into boiling DI water for 5 hours in order to get rid of the LiCl. Finally, the membranes were placed into the oven at 190 °C for 3 hours to dry and completely eliminate the residual DMAc.

3.3.1 PBI/MWCNT membrane preparation

PBI/MWCNT membranes were prepared using the same method mentioned above. However, before casting the solutions into the petri dishes, MWCNTs were added (0.5wt% and 1wt%) and ultrasonically homogenised in an ice bath for 6 hours for a complete dispersion (at 10% power, to not to damage the nanotubes). Then the solutions were cast into the petri dishes. Figure 3.5 shows the dry membranes before the acid doping.

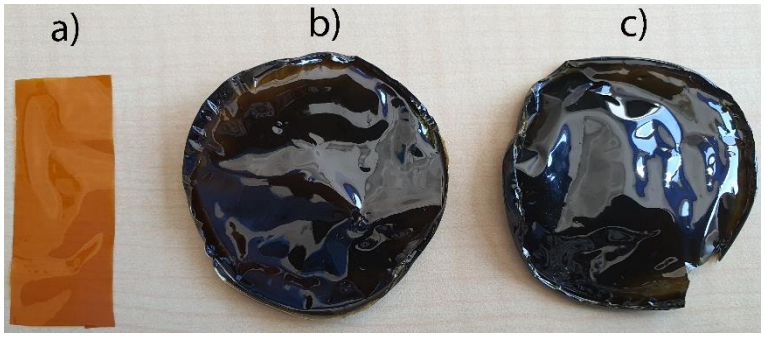

Figure 3.5: Undoped a) Pristine PBI membrane, b) 0.5wt% PBI/MWCNT membrane, c) 1wt% PBI/MWCNT membrane.

3.3.2 Acid doped membrane preparation

For acid doping process, the membranes were put into o-phosphoric acid (PA, H_3PO_4, 85%) acid for 5 days at room temperature. After 5 days, the membranes were taken

from the acid and dried with paper towels to get rid of the excess acid. Then they were dried at 90 °C in vacuum for 5 hours to eliminate the water uptake effect for acid doping calculations. The method to find the moles of phosphoric acid per mol of PBI repeat unit is given in equation (3.1).

$$Acid\ Doping = \frac{weight\ difference}{initial\ weight} . \frac{M_W\ of\ mPBI\ repeat\ unit}{M_W\ of\ H_3PO_4} \quad (3.1)$$

In this equation, M_W of mPBI repeat unit is 308 g/mol, and M_W of H_3PO_4 is 98 g/mol. Figure 3.6 shows the membranes after the acid doping.

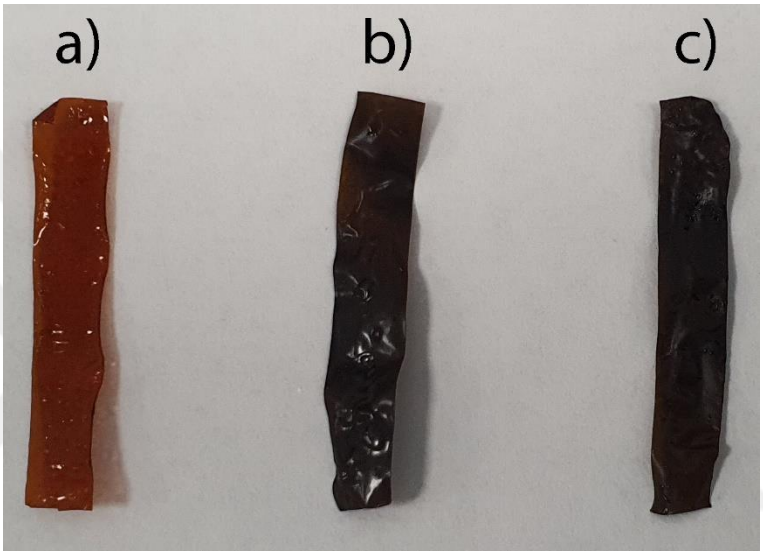

Figure 3.6: Doped a) Pristine PBI membrane, b) 0.5wt% PBI/MWCNT membrane, c) 1wt% PBI/MWCNT membrane.

3.4 Characterisation

3.4.1 Nuclear magnetic resonance spectroscopy (NMR) analysis

The nuclear magnetic resonance spectroscopy (NMR) of pristine PBI polymer was conducted at room temperature via 1H-NMR using Agilent VNMRS 500 MHz. The solution was DMSO-d6.

3.4.2 Thermogravimetric analysis (TGA)

The weight loss of both doped and undoped membranes were conducted via TGA analyses. The tests were conducted between room temperature to 600 °C for the undoped membranes and the ground PBI polymer with an increase rate of 5 °C/min. For the doped membranes, the tests were conducted from room temperature to 200 °C

with an increase rate of 2 °C/min and kept at 200 °C for 2 hours. The test atmosphere was nitrogen.

3.4.3 X-Ray diffraction (XRD) analysis

XRD analyses of undoped membranes were made by using Philips PW 3710. The anode was set to 40 kV, 40 mA, and the radiation was CuKα λ = 1.5406 Å. The angle sweep was 0.02°/second between 10°-80°.

3.4.4 Fourier transform infrared spectroscopy (FT-IR) analysis

For FT-IR analyses for both doped and undoped membranes, PerkinElmer Spectrum 100 FT-IR was used. The analyses were performed between the wavenumbers 4000-650 cm^{-1}.

3.4.5 Scanning electron microscopy (SEM) analysis

SEM analyses for both doped and undoped membranes were performed by using FEI Quanta 250 FEG. The membranes were coated with Au/Pd before the observation process. Then they were placed in the SEM to investigate the MWCNT distribution and the effect of acid doping.

3.4.6 Electrochemical impedance spectroscopy (EIS) analysis

The ionic in-plane conductivities of the doped membranes were measured by Gamry 1010E potentiostat with the potentiostatic EIS test, using the two-probe method. The frequency range for the tests was 1 MHz to 1 Hz, 10 points/decade, 100 mV_{AC} at 0 V_{DC} (vs E_{OC}). The dimensions of the membranes were w_m = 7 mm wide, l_m = 38 mm long and t_m = 85 µm thick for the pristine PBI membrane, w_m = 65 mm wide, l_m = 37 mm long and t_m = 119 µm thick for the 0.5wt% MWCNT/PBI membrane and w_m = 6 mm wide, l_m = 36 mm long and t_m = 67 µm thick for the 1wt% MWCNT/PBI membrane. The membranes were placed in a Teflon conductivity cell, containing four Pt electrodes. The distance between each electrode is 10 mm, but 20 mm was also used for the measurements as D in equation (2.29). Figure 3.7 shows the conductivity cell.

The resistances of the membranes at 120 °C, 140 °C and 160 °C obtained via Nyquist plot. After that, the conductivity values of the membranes were calculated by using the equation (2.29).

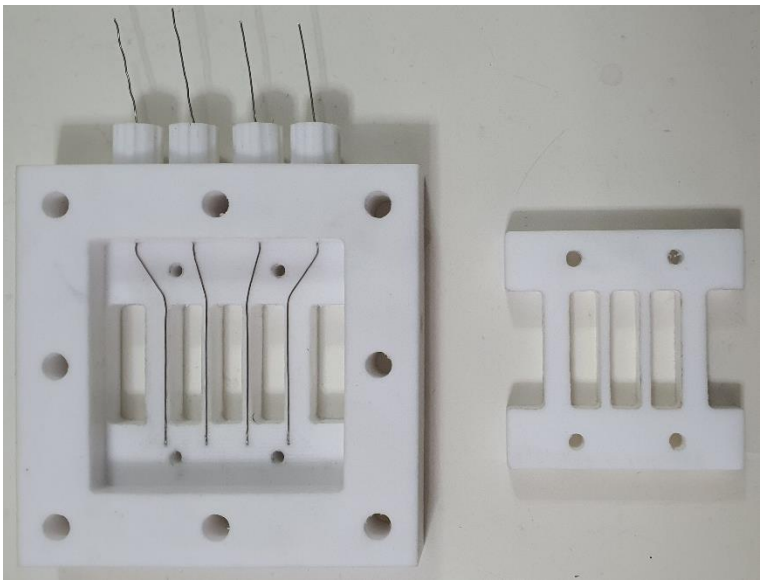

Figure 3.7: The conductivity cell.

The measurements were taken at the time stamps of 40 and 60 minutes and compared. There were no differences between the two periods. So, before measuring in the specified temperatures, 40 minutes passed each time to ensure the thermal stability. Figure 3.8 shows the cell assembly.

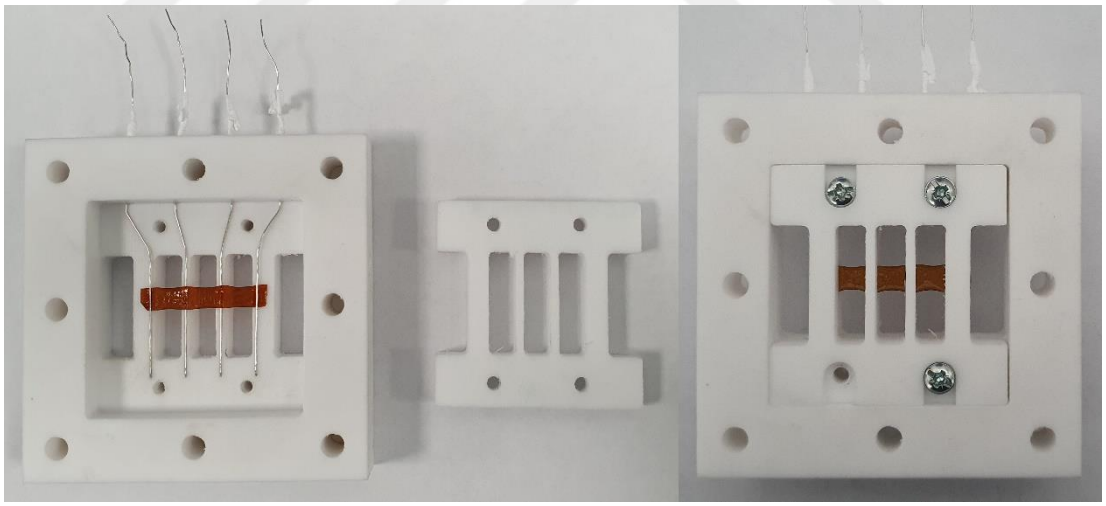

Figure 3.8: The complete cell with the doped membrane.

In order to maintain the high temperatures, a homemade test system was built. A small (big enough for the cell to fit) stainless steel pot was purchased. The lid of the pot was drilled in a milling cutter according to the cell, 4 holes for the electrodes, 5.5 mm in diameter each and 1 hole for the thermocouple, 7 mm in diameter, as shown in Figure 3.9.

The electrodes and the thermocouple were covered with a thick layer of ptfe tape in

Figure 3.9: The drilled pot lid.

order to break the contact of the electrodes with the lid, as well as the thermocouple and the lid. After that, the cell was placed into the pot and the pot was placed onto the magnetic stirrer and heater. The thermocouple of the stirrer was placed in the pot and the pot was covered with rock wool within an aluminium foil to maintain the thermal isolation and the stability. Figure 3.10 shows the cell placement in the pot.

Figure 3.10: The cell placement in the pot.

Finally, the probes were connected to the potentiostat with crocodile holders. For the two-probe measurement, the working and the working sense electrodes were connected serially (shorted) to one probe, then the reference and the counter electrodes were connected serially (shorted) to the other probe. Figure 3.11 shows the final experimental setup.

Figure 3.11: The experimental setup for the impedance measurements.

4. RESULTS AND DISCUSSION

4.1 PBI Polymer Synthesis Results

The PBI polymer was synthesised according to solution polymerisation method. The intrinsic viscosity (η_{int}) should be at least 1.3 dl/g (1 dl = 100 ml) for good mechanical stability. The reaction took 24 hours with a slow mixing speed to ensure the high intrinsic viscosity, thus higher molecular weight, in order to achieve a strong membrane that can endure higher acid doping levels. Higher mixing speeds decrease the viscosity. It is crucial for mixing speed to be low and the reaction rate to be at least 17-24 hours to obtain high molecular weight PBI polymer.

4.1.1 Nuclear magnetic resonance (NMR) spectroscopy analysis results

The 1H-NMR result of the PBI polymer is given in Figure 4.1. The synthesis procedure took 24 hours at 200 °C, around 150 rpm mixing rate.

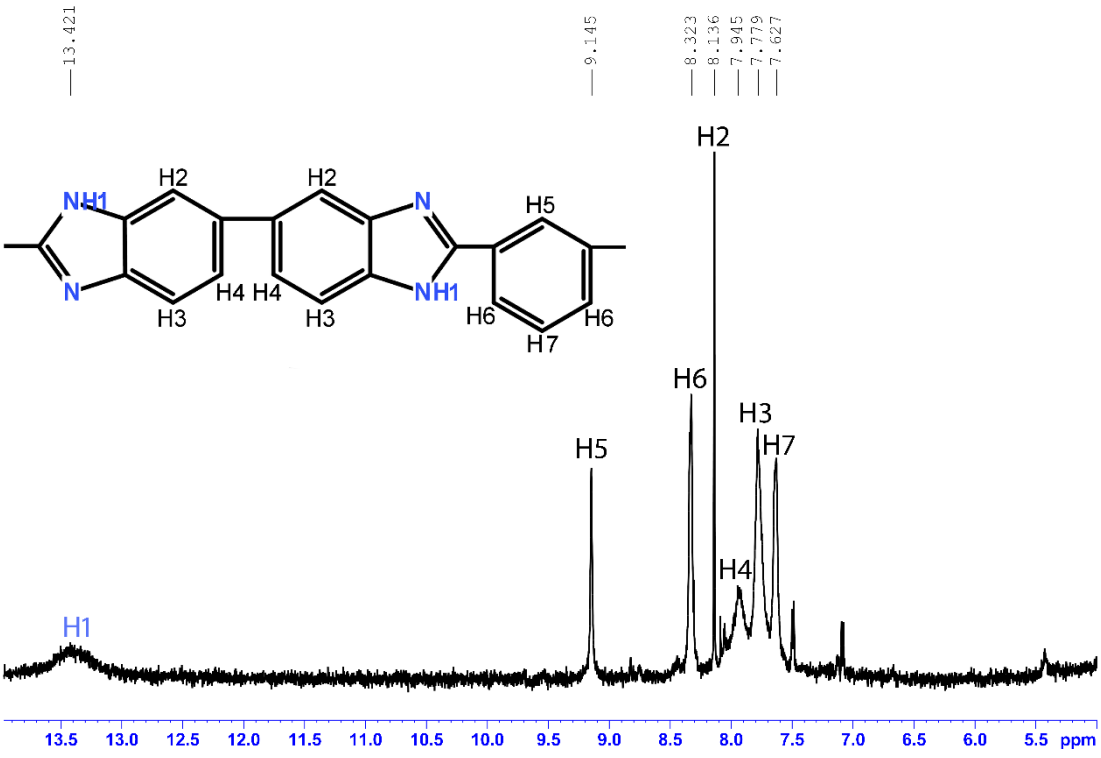

Figure 4.1: 1H-NMR results of the synthesised PBI polymer.

In this figure, the peak at 13.421 ppm indicates H1, which is the imidazole protons [55]. Other peaks, which are located between 9.2 ppm and 7.5 ppm are the aromatic protons. H2, H3 and H4 are represented with 8.136 ppm, 7.779 ppm and 7.945 ppm, respectively. H5, H6 and H7 are located on 9.145 ppm, 8.323 ppm and 7.627 ppm, respectively. Small peaks may be due to the impurities within the PBI powder. They may be the result of unused reactants and/or impurities caught in the post-processing of PBI polymer.

4.2 Membrane Preparation Results

The membranes were prepared by using the solution casting method. The polymer was dissolved in DMAc without a need of inert atmosphere. That is because the lower temperature used while dissolving it. At higher temperatures, oxygen may interact with the solution and cause a gel formation, as well as cross-linking. However, lower temperatures (around 70-80 °C) can easily dissolve PBI in DMAc, without a need of an inert atmosphere. A simple ptfe stirrer was used for the procedure. And the absence of the precipitation at the end of the centrifuge process showed that the polymer dissolved completely. The centrifuge process also helped with the elimination of possible gas bubbles and undesired residue, such as dust, within the solution for the casting.

4.2.1 PBI/MWCNT membrane preparation results

After the PBI polymer was dissolved in DMAc and centrifuged, 0.5wt% and 1wt% MWCNTs were prepared and added to the solutions. To ensure the complete dispersion of the nanotubes for the casting method, homogeniser is essential. Ice bath was used to lower the temperature of the solution, because the ultrasonic homogeniser heats the solution to high temperatures and PBI dries on the surface of the ultrasonic probe, as well as the beaker (centrifuge tube in our case). The ice bath was changed every hour. At the end of the process, fully dispersed PBI/MWCNT mixtures were easily obtained for membrane casting.

4.2.2 Acid doped membrane preparation results

The membranes were kept in the 85% acid for 5 days. The doping levels were calculated as 14.3 mol PA/PBI for the pristine PBI, 5.9 mol PA/PBI for the 0.5wt%

MWCNT/PBI membrane and 7.3 mol PA/PBI for the 1wt% MWCNT/PBI membrane. It was seen that adding MWCNTs increases the acid uptake for the composite membranes due to the retention of the acid to the MWCNTs; which is appropriate with the literature [47]. Table 4.1 shows the acid doping results.

Table 4.1: The acid doping results of the membranes.

Membrane	Acid Doping Level (mol PA/PBI)
Pristine PBI	14.3
0.5wt% PBI/MWCNT	5.9
1wt% PBI/MWCNT	7.3

4.2.3 Thermogravimetric analysis (TGA) results

The thermal stability tests were conducted via TGA. For the undoped membranes, the first decrease in weight, until around 150 °C, is due to the water evaporation. It is common in all the membranes and the ground polymer. Then, a significant weight loss was observed around 550 °C, which indicates that the decomposition started at this point. Until 550 °C there is no significant weight loss, which means the polymer has excellent thermal stability. The weight loss between 220-420 °C is attributed to the decomposition of PBI coated MWCNTs [56]. Since this temperature is out of HT-PEM operating temperature, these membranes can be used in the cells. Figure 4.2 shows the TGA results of the undoped membranes and ground PBI polymer.

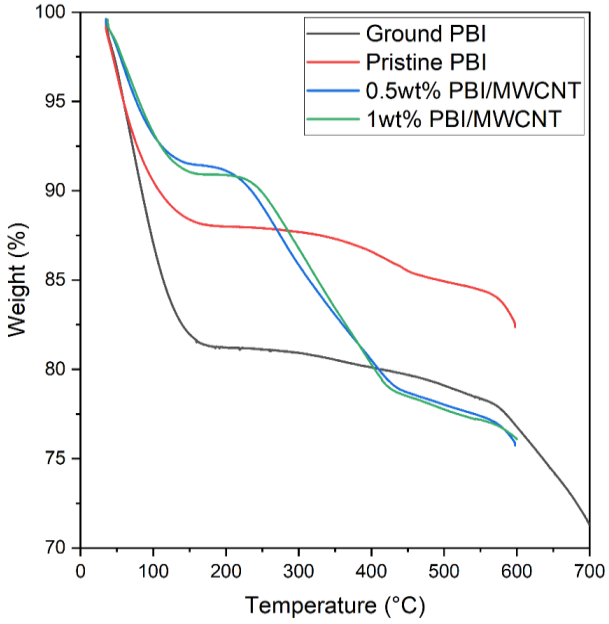

Figure 4.2: TGA results of the undoped membranes.

The doped membranes were tested after the EIS tests. In the Figure 4.3, the weight losses up to 100 °C, which is due to the water evaporation. The loss between 120 °C and 200 °C is due to the acid dehydration. Phosphoric acid dehydrates to pyrophosphoric acid, and then to triphosphoric acid. However, this process is reversible and acid regains the water in the humid medium at lower temperatures. There were no decompositions observed. All the membranes are fit to use in fuel cell applications.

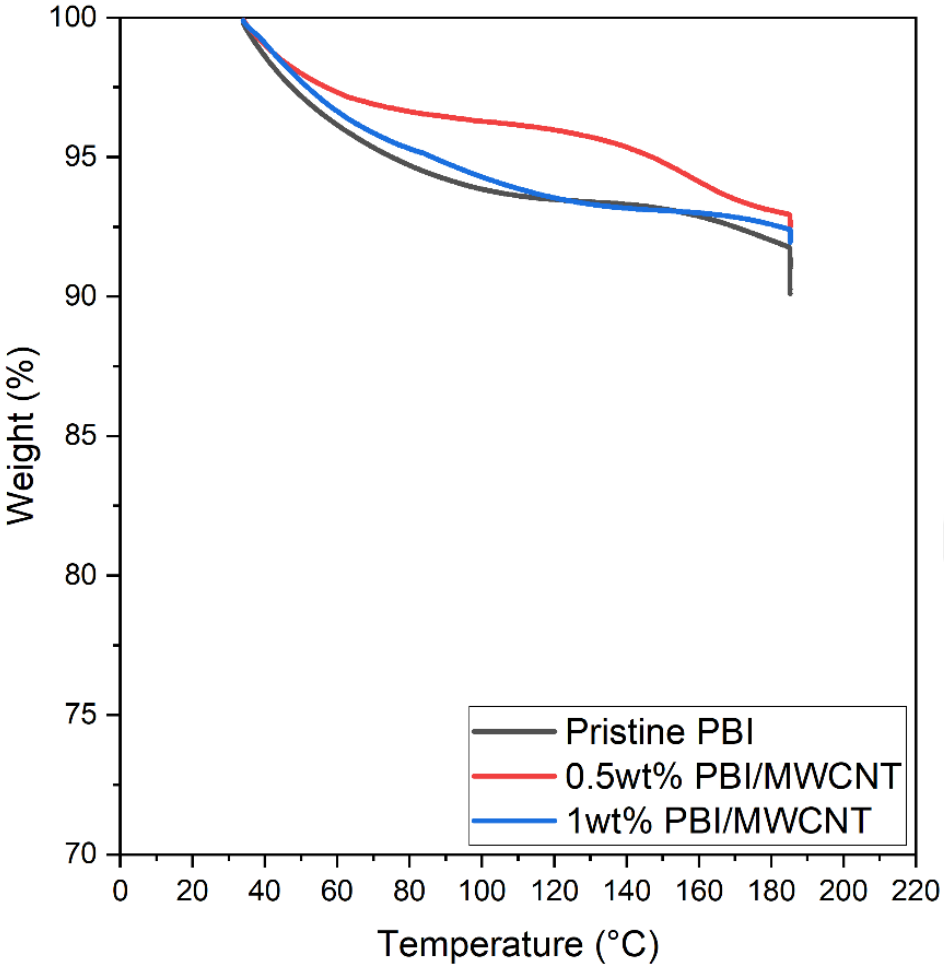

Figure 4.3: TGA results of the doped membranes.

4.2.4 X-Ray diffraction (XRD) analysis results

The results of the XRD analyses of undoped PBI membranes is given in Figure 4.4. It can be seen from the figure that the broad peaks are at $2\theta = 25°$, which is due to the semi-crystalline structure of the PBI membranes. A small increase in the intensity of the peak is observed with the increasing MWCNT content, as expected because of the carbon's peak, which is also around $2\theta = 25°$. The results are in good agreement with the literature [48].

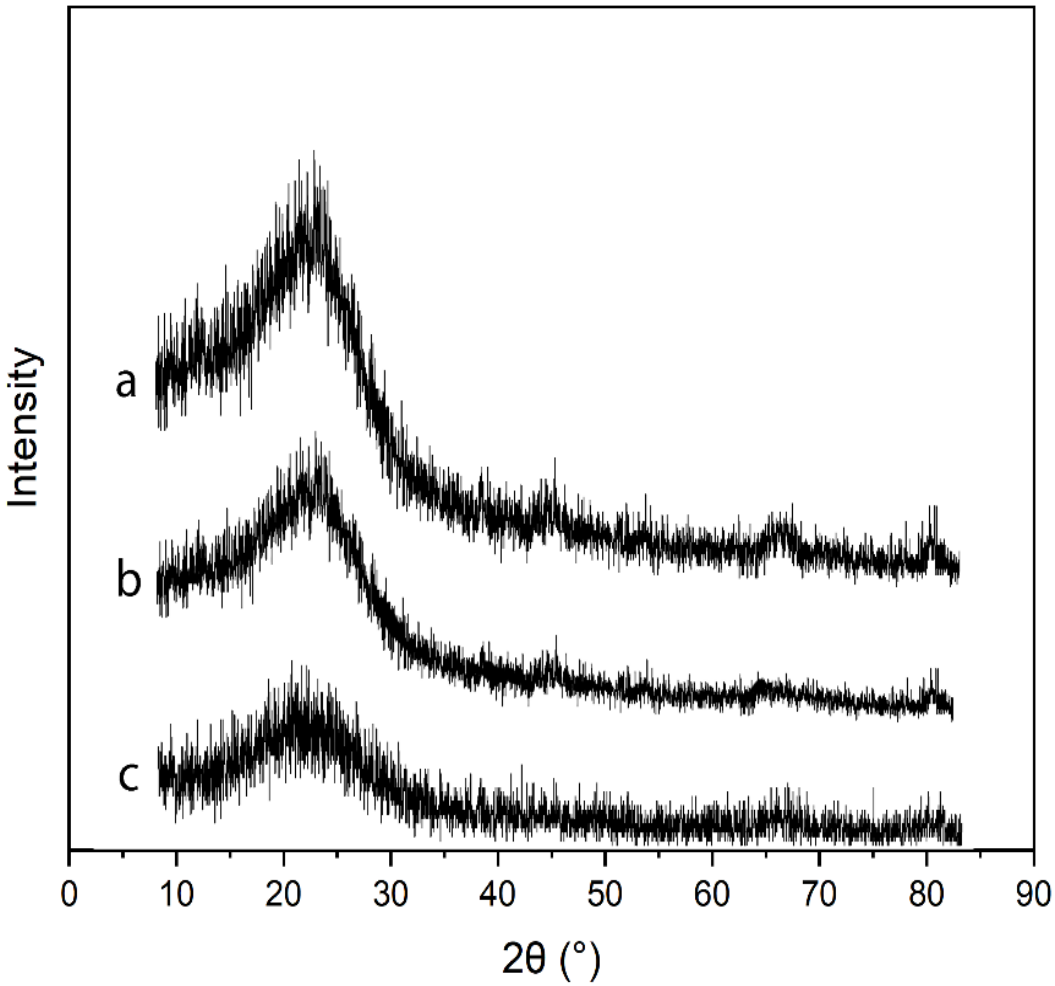

Figure 4.4: XRD results of the membranes. a is 1wt% PBI/MWCNT, b is 0.5wt% PBI/MWCNT and c is pristine PBI.

4.2.5 Fourier transform infrared (FT-IR) spectroscopy analysis results

Figure 4.5 shows the FT-IR spectra. According to FT-IR results, the peaks between 4000-2000 cm^{-1} are attributed to the N-H stretching and 1000-1700 cm^{-1} are attributed to the benzene/imidazole rings [47]. The peaks of the membranes are around 1620, 1530, 1440, 1280 and 790 cm^{-1}. These peaks mean strong C=C/C=N stretch, the characteristic of 2-substitution, the characteristic of benzimidazole in plane vibration, C-N stretch and C-H bending, respectively. The peak around 2920 cm^{-1} shows the N-H group. Narrow peaks below 2000 cm^{-1} belong to phenyl groups.

It can be seen that the acid doping drastically changed the bonds within the polymer. C-N, H-N and cycle deformations occur between 2000-1000 cm^{-1}. The effect of the phosphoric acid uptake greatly influences the visibility of the peaks due to the hydrogen bonding, as well as vibrations of hydrogen phosphate groups. Acid doping introduces a new peak at 1495 cm^{-1}, which is related to the C=N vibrations of the

$C=NH^+$ group and caused by the protonation of imino nitrogen atom. The broad band between 2500-3000 cm^{-1} is related to the protonation of the nitrogen of the imide, resulted by the proton transfer from phosphoric acid to imidazole groups in PBI, which means bonded acid [57].

For the composite membranes, the absorption bands of CNTs are indistinguishable due to the non-covalent π-π interactions between the polymer and the CNTs. For the doped composite membranes, the peaks around 1080 and 870 cm^{-1} are attributed to the phosphoric acid dissociation [47].

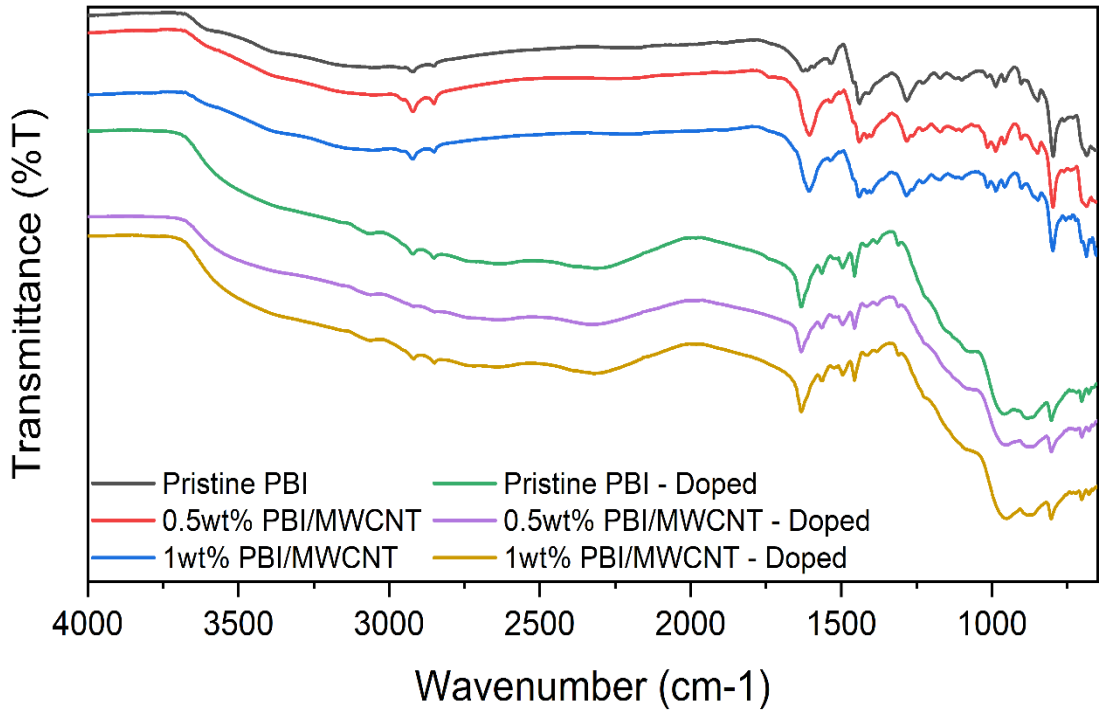

Figure 4.5: The FT-IR results of the membranes.

4.2.6 Scanning electron microscopy (SEM) analysis results

Figure 4.6 shows the morphological structure of the membranes. In Figure 4.6c, the tips of the MWCNTs can be clearly seen as white dots. The uniform dispersion of these dots, as well as individually and randomly, indicates a good dispersion, along with the absence of lumps.

The pictures of the membranes are taken with different zoom levels. It is almost impossible to see the MWCNTs unless it is 1 μm or a smaller number. That is why pristine PBI, 0.5wt% PBI/MWCNT and doped membranes seem empty while 1wt% PBI/MWCNT displays a good vision.

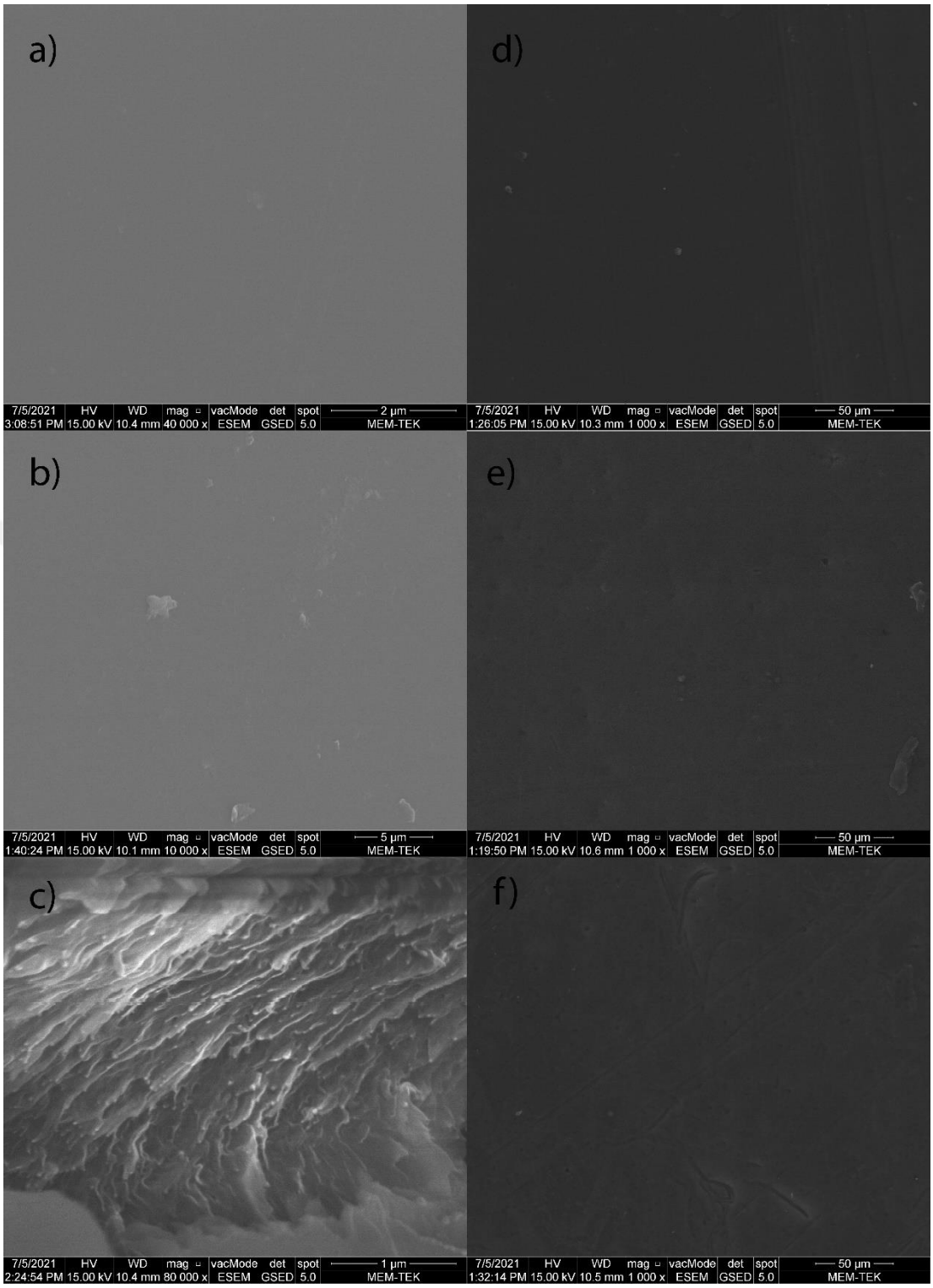

Figure 4.6: The SEM pictures of the membranes. a) Pristine PBI, b) 0.5wt% PBI/MWCNT, c) 1wt% PBI/MWCNT, d) doped Pristine PBI, e) doped 0.5wt% PBI/MWCNT, f) doped 1wt% PBI/MWCNT

4.2.7 Electrochemical impedance spectroscopy (EIS) analysis results

The impedance measurements of the membranes were carried out in anhydrous conditions and their conductivities were calculated. The measurements of the pristine

PBI membrane were taken with two different probe distances, 1 cm and 2 cm. The comparison of the impedance measurement results of the pristine PBI membrane at 160 °C is given in Figure 4.7.

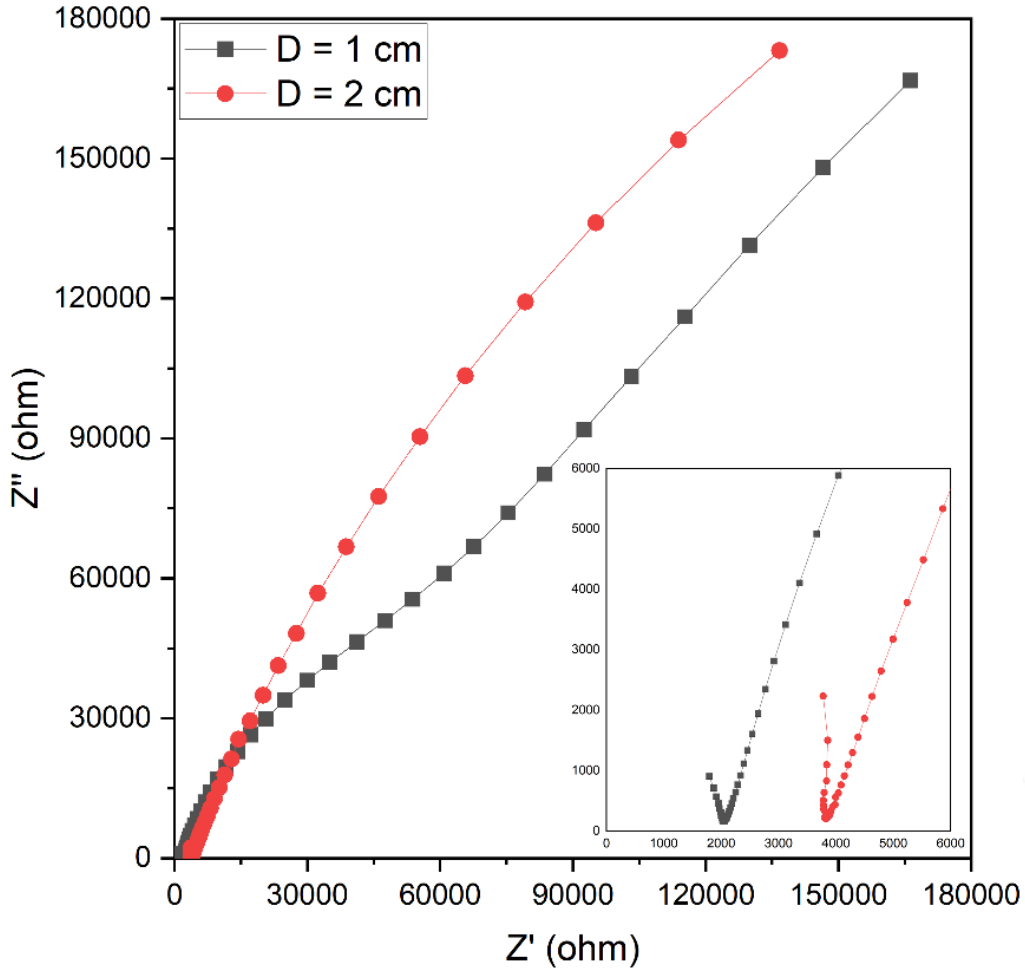

Figure 4.7: The comparison of the probe distance D at 160 °C.

These results were fitted with different equivalent circuits. Model 1 is from [53] and model 2 is a circuit derived from the fuel cell circuit. All the given circuits are simplifications of the given circuit in Figure 2.9. The experimental data of the 1 cm measurement, its fits and the equivalent circuits of the fits are given in the Figure 4.8. In these models, R_b and C_b are the bulk resistance and the capacitance of the membrane, respectively. CPEs are the constant phase elements, which are better representations of the capacitances, due to their correction value of the non-homogeneity. CPE_{dl} is the polarisation capacitance of the membrane and CPE_b is used instead of the bulk capacitance. According to the experimental data and the fit models, the conductivities are 0.08885 S/cm, 0.08165 S/cm and 0.08438 S/cm for experimental, model 1 and model 2, respectively.

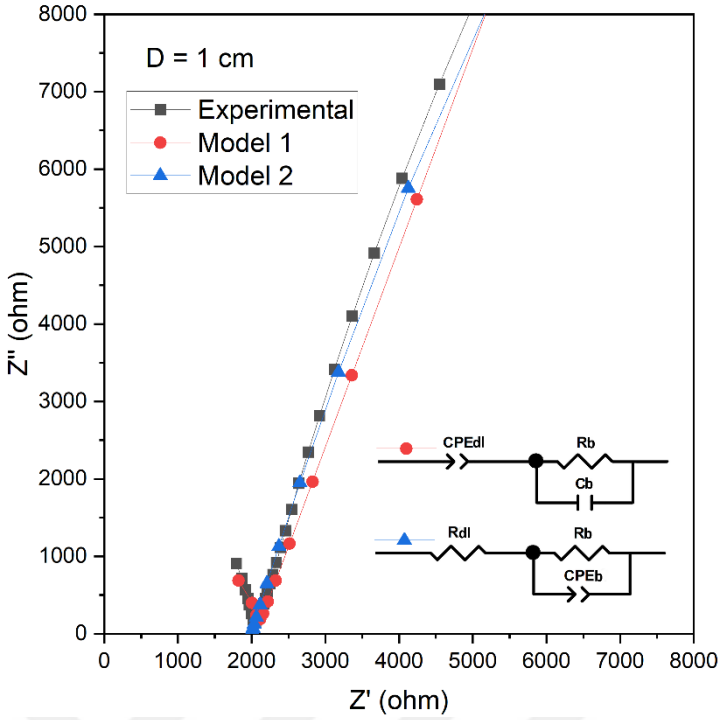

Figure 4.8: D = 1 cm measurement at 160 °C and its equivalent circuits.

Figure 4.9 shows the results of the 2 cm distance measurements under the same conditions and its equivalent circuits. According to the experimental data and the fit models, the conductivities are 0.0895 S/cm, 0.0865 S/cm and 0.0879 S/cm for experimental, model 1 and model 2, respectively.

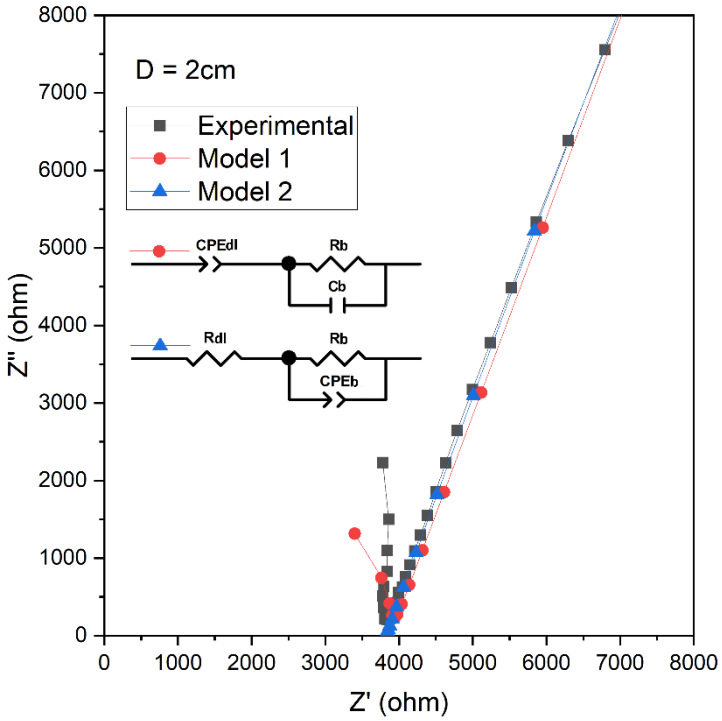

Figure 4.9: D = 2 cm measurement at 160 °C and its equivalent circuits.

It is known that increasing the probe distance between the voltage probes gives more reliable results, due to the sharp separation between the interfacial and bulk impedances as a result of the shift to the low-frequency region of the characterisation frequency [58]. Figure 4.10 shows the conductivity comparison of the experimental data and the fits.

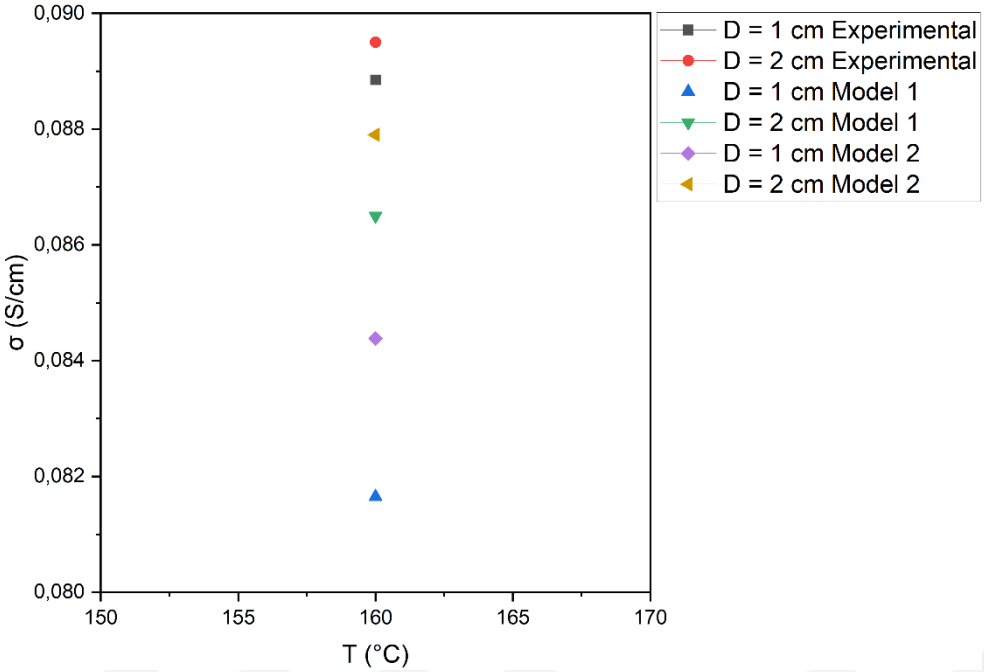

Figure 4.10: Conductivity results of the measurements and their fits at 160 °C.

As seen in the graphic, the equivalent circuit of model 2 yielded better results than model 1. However, both models can be accepted and used, since the difference is insignificant. Table 4.2 shows the results of the measurements and the fits. Although great differences were not observed between the measurements, the rest of the results are given according to the 2 cm distance.

Table 4.2: The conductivity results of the EIS measurements and their equivalent circuits at 160 °C.

Data Type	Conductivity, σ (S/cm)	
	D = 1 cm	D = 2 cm
Experimental	0.08885	0.0895
Model 1	0.08165	0.0865
Model 2	0.08438	0.0879

After the measurements at 120 °C, 140 °C and 160 °C with a 100 mV V_{AC}, the conductivities of the pristine PBI membrane were calculated as 0.0518 S/cm, 0.0667

S/cm and 0.0895 S/cm, respectively. These values are in good agreement with the literature, except 160 °C, which is a bit higher than the literature, yet still acceptable.

The conductivities of composite membranes are consistent in itself. An increase in the ionic conductivities is expected, in regards to the increasing MWCNT content. The conductivities of the 0.5wt% PBI/MWCNT membrane is 0.0401 S/cm, 0.0586 S/cm and 0.0613 S/cm for 120 °C, 140 °C and 160 °C, respectively. As expected from 1wt% PBI/MWCNT membrane, slightly higher conductivities were obtained. The temperatures 120 °C, 140 °C and 160 °C yielded 0.0429 S/cm, 0.0621 S/cm and 0.0655 S/cm, respectively. Because the acid doping level is higher for the pristine PBI membrane, a true comparison cannot be made for the protonic conductivities. Figure 4.11 shows the EIS results of the membranes. Figure 4.12 and Table 4.3 show the conductivities of all the membranes.

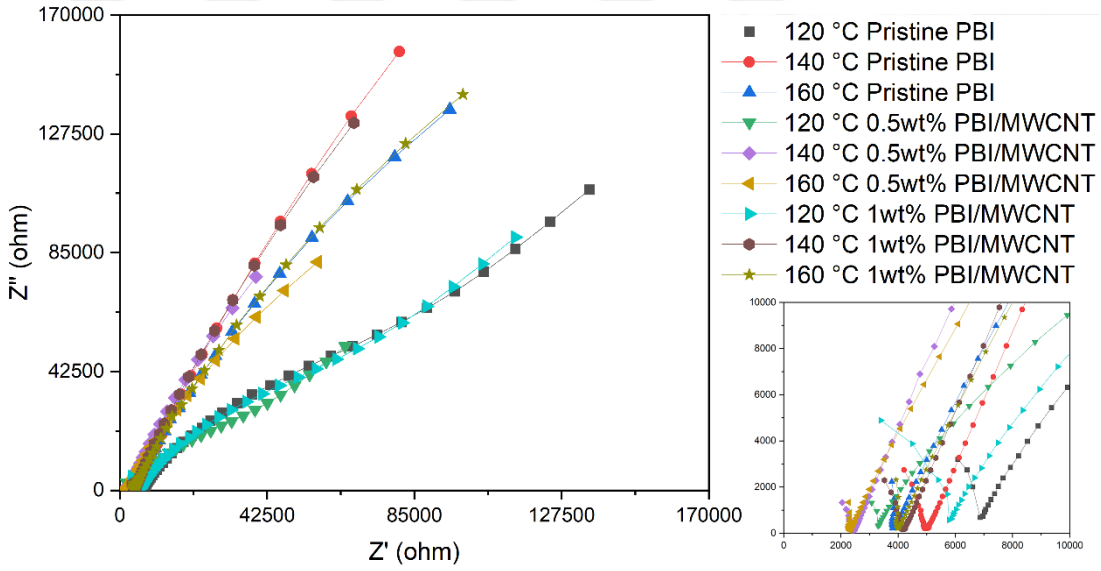

Figure 4.11: EIS results of the membranes.

Table 4.3: The conductivity results of the membranes.

Temperature, T (°C)	Conductivity, σ (S/cm)		
	Pristine PBI	0.5wt% PBI/MWCNT	1wt% PBI/MWCNT
120	0.0518	0.0401	0.0429
140	0.0667	0.0586	0.0621
160	0.0895	0.0613	0.0655

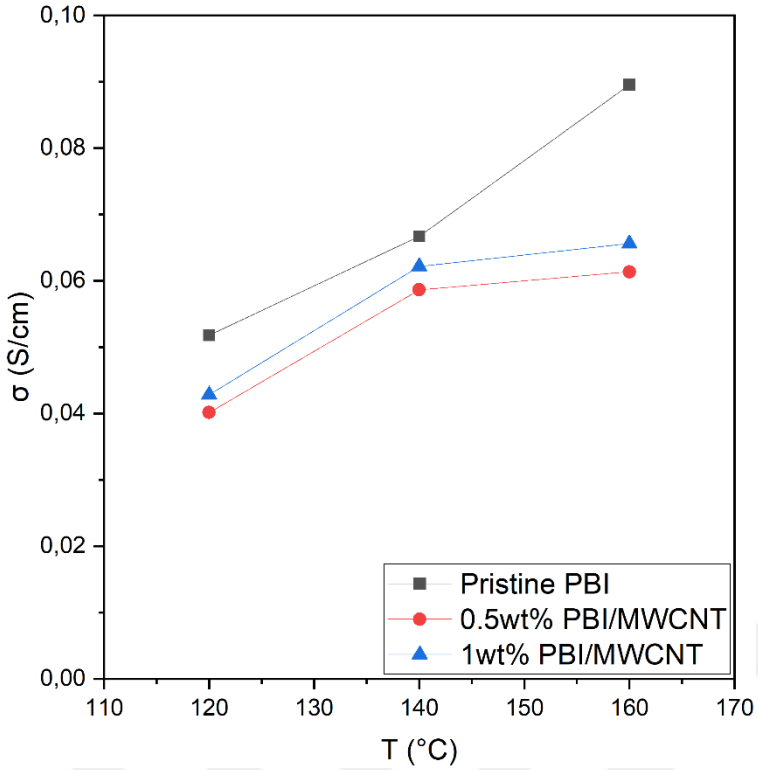

Figure 4.12: The conductivities of the membranes.

5. CONCLUSIONS AND RECOMMENDATIONS

5.1 Conclusions

The aim of the study was to investigate the effect of MWCNT loading in the PBI membrane. Thus, PBI membranes were prepared as pristine and MWCNT-supported. The effect of different amounts of MWCNT loadings were studied. We had to use only one set of samples in the tests. Due to The Corona Virus Pandemic, our DAB.4HCl was expired in the first stage of the lockdown, when we could not reach to our laboratory between 16th of March and 1st of July 2020. We tried to synthesise PBI polymer after this for 6 months (until January 2021) but all of them failed. We decided to check the chemicals in 1H-NMR to see if there was something wrong, and that was when we saw that our DAB.4HCl was expired. After that, we could not get another one. That is why, the calculations and measurements were made only on one set of samples.

The PBI polymer was synthesised via solution polymerisation method and characterised for the HT-PEMFC applications. It was first characterised by NMR and FT-IR. The peaks, which belonged to PBI, were observed clearly in both tests. Combined with the result of the TGA, it was concluded that the synthesised material was indeed PBI.

The synthesised polymer was dissolved in the DMAc, in order to obtain mechanically strong and thermally stable PBI membranes by casting method. The membranes were then further characterised by TGA and XRD. TGA yields an exceptional thermal stability, up to 550 °C and MWCNTs have no effect on the decomposition temperature. XRD results showed the semi-crystalline structure of the polymer.

The acid doping results showed an interesting case. Although 48 hours in the room temperature is enough to obtain saturated membranes, 5 days was necessary because of our laboratory conditions. After 2 days, the membranes were taken from the acid and dried in the oven to calculate the acid doping level. It was seen that the acid doping was 3.14 mol PA/PBI for all the membranes. At this point we realised that a window

was open in the lab the whole time, so the room temperature was not achieved. So, we kept the membranes in the acid for 3 more days in our rooms. The pristine PBI membrane has a higher acid doping level. This may be attributed to the swelling of the membrane because of the first acid doping process. In the first drying process, the evaporating water may have created small air bubbles within the membrane. So, the swollen pristine PBI membrane may have had more room for free acid, which could be absorbed in the second doping. Another explanation could be made as the residual excess acid. After the second doping, there might be some acid left on the membrane even after drying it with paper towels, which could increase the doping level in the oven at 90 °C. No other comments could be made on the subject, because all the membranes were in the same acid container the whole time and they were dried together.

The surface morphology and the dispersion of the MWCNTs were also observed. It was seen that the ultrasonic homogenisation resulted in highly well dispersed MWCNTs within the membrane. It was also seen that the MWCNT-support increased the acid doping level for the composite membranes due to the acid retention. The EIS results exhibited an increase in the protonic conductivity for all membranes with the increasing temperature. MWCNT-support also showed an increase in the protonic conductivity within itself when the 0.5 and 1wt% MWCNT/PBI membranes were compared to one another.

Consequently, pristine and MWCNT-supported membranes were prepared and investigated. High conductivities comparable to Nafion were obtained [59,60].

5.2 Recommendations

The recommendations for further investigations can be made as follows:

- Membranes with exact same acid doping levels can be prepared and compared in order to get a better understanding on the effect of MWCNT-support on tensile strength and protonic conductivity.
- The MWCNTs can be functionalised in order to increase the acid retention and protonic conduction.
- Membranes can be fabricated by using screen printing or spin coating methods in order to increase homogeneity of the films.

- Performance tests can be made in a fuel cell testing system to investigate the effects of MWCNTs in a working cell.
- Membranes with different support materials can be prepared and compared.

REFERENCES

[1] **DLR - Institute of Combustion Technology - Hybrid Power Plant.** (2019). Deutsches Zentrum Für Luft- Und Raumfahrt (German Aerospace Centre). https://bit.ly/3t7KRyR Last Access: 13.07.2021

[2] **Sorrell, C. C., Nowotny, J., & Sugihara, S.** (2005). Materials for Energy Conversion Devices (Woodhead Publishing Series in Electronic and Optical Materials) (1st ed.). Woodhead Publishing.

[3] **Barbir, F.** (2012). PEM Fuel Cells: Theory and Practice (2nd ed.). Academic Press.

[4**] Korn, M.** (2020, December 14). Are hydrogen fuel cell vehicles the future of autos? ABC News. https://abcn.ws/2OFls0I Last Access: 13.07.2021

[5] **Mench, M. M.** (2008). Fuel Cell Engines (1st ed.). Wiley.

[6] **Zhang, J.** (2008). PEM Fuel Cell Electrocatalysts and Catalyst Layers: Fundamentals and Applications (2008th ed.). Springer.

[7] **Wainright, J. S., Wang, J. T., Weng, D., Savinell, R. F., & Litt, M.** (1995). Acid-Doped Polybenzimidazoles: A New Polymer Electrolyte. Journal of The Electrochemical Society, 142(7), L121–L123. https://doi.org/10.1149/1.2044337

[8] **Li, Q., He, R., Jensen, J., & Bjerrum, N.** (2004). PBI-Based Polymer Membranes for High Temperature Fuel Cells– Preparation, Characterization and Fuel Cell Demonstration. Fuel Cells, 4(3), 147–159. https://doi.org/10.1002/fuce.200400020

[9] **Li, Q., Jensen, J. O., Savinell, R. F., & Bjerrum, N. J.** (2009). High temperature proton exchange membranes based on polybenzimidazoles for fuel cells. Progress in Polymer Science, 34(5), 449–477. https://doi.org/10.1016/j.progpolymsci.2008.12.003

[10] **Søndergaard, T., Cleemann, L. N., Becker, H., Steenberg, T., Hjuler, H. A., Seerup, L., Li, Q., & Jensen, J. O.** (2018). Long-Term Durability of PBI-Based HT-PEM Fuel Cells: Effect of Operating Parameters. Journal of The Electrochemical Society, 165(6), F3053–F3062. https://doi.org/10.1149/2.0081806jes

[11] **Søndergaard, T., Cleemann, L. N., Becker, H., Aili, D., Steenberg, T., Hjuler, H. A., Seerup, L., Li, Q., & Jensen, J. O.** (2017). Long-term durability of HT-PEM fuel cells based on thermally cross-linked polybenzimidazole. Journal of Power Sources, 342, 570–578. https://doi.org/ 10.1016/j.jpowsour.2016.12.075

[12] **Chen, J., Perez-Page, M., Ji, Z., Zhang, Z., Guo, Z., & Holmes, S.** (2021). One step electrochemical exfoliation of natural graphite flakes into graphene oxide for polybenzimidazole composite membranes giving enhanced performance in high temperature fuel cells. Journal of Power Sources, 491, 229550. https://doi.org/10.1016/j.jpowsour.2021.229550

[13] **Kumar, S. R., Wang, J. J., Wu, Y. S., Yang, C. C., & Lue, S. J.** (2020). Synergistic role of graphene oxide-magnetite nanofillers contribution on ionic conductivity and permeability for polybenzimidazole membrane electrolytes. Journal of Power Sources, 445, 227293. https://doi.org/ 10.1016/j.jpowsour.2019.227293

[14] **Brinker, K. C., & Robinson, I. M.** (1959). Polybenzimidazoles (2,895,948). United States Patent Office. https://patents.google.com/ patent/US2895948A/en

[15] **Vogel, H., & Marvel, C. S.** (1960). Polybenzimidazoles, New Thermally Stable Polymers. Journal of Polymer Scıence, L, 511–539. https://doi.org/ 10.1002/pol.1961.1205015419

[16] **Olabisi, O., & Adewale, K.** (2015). Handbook of Thermoplastics (Plastics Engineering) (2nd ed.). CRC Press.

[17] **Iwakura, Y., Uno, K., & Imai, Y.** (1964). Polyphenylenebenzimidazoles. Journal of Polymer Science Part A: General Papers, 2(6), 2605–2615. https://doi.org/10.1002/pol.1964.100020611

[18] **Zeis, R.** (2015). Materials and characterization techniques for high-temperature polymer electrolyte membrane fuel cells. Beilstein Journal of Nanotechnology, 6, 68–83. https://doi.org/10.3762/bjnano.6.8

[19] **Salamone, J. C.** (2020). Polymeric Materials Encyclopedia, Twelve Volume Set, Volume 7 (1st ed.). CRC Press.

[20] **Du, H. Y., Yang, C. S., Hsu, H. C., Huang, H. C., Chang, S. T., Wang, C. H., Chen, J. C., Chen, K. H., & Chen, L. C.** (2015). Pulsed electrochemical deposition of Pt NPs on polybenzimidazole-CNT hybrid electrode for high-temperature proton exchange membrane fuel cells. International Journal of Hydrogen Energy, 40(41), 14398–14404. https://doi.org/ 10.1016/j.ijhydene.2015.04.131

[21] **Kaewsai, D., Lin, H. L., Liu, Y. C., & Yu, T. L.** (2016). Platinum on pyridine-polybenzimidazole wrapped carbon nanotube supports for high temperature proton exchange membrane fuel cells. International Journal of Hydrogen Energy, 41(24), 10430–10445. https://doi.org/ 10.1016/j.ijhydene.2015.09.066

[22] **Eren, E. O., Özkan, N., & Devrim, Y.** (2020). Polybenzimidazole-modified carbon nanotubes as a support material for platinum-based high-temperature proton exchange membrane fuel cell electrocatalysts. International Journal of Hydrogen Energy, In Press. https://doi.org/ 10.1016/j.ijhydene.2020.07.101

[23] **Haque, M., Sulong, A., Shyuan, L., Majlan, E., Husaini, T., & Rosli, R.** (2021). Synthesis of polymer/MWCNT nanocomposite catalyst supporting materials for high-temperature PEM fuel cells. International Journal of Hydrogen Energy, 46(5), 4339–4353. https://doi.org/10.1016/j.ijhydene.2020.10.200

[24] **Gebremariam, T. T., Chen, F., Kou, B., Guo, L., Pan, B., Wang, Q., Li, Z., & Bian, W.** (2020). PdAgRu nanoparticles on polybenzimidazole wrapped CNTs for electrocatalytic formate oxidation. Electrochimica Acta, 354, 136678. https://doi.org/10.1016/j.electacta.2020.136678

[25] **Ergun, D., Devrim, Y., Bac, N., & Eroglu, I.** (2012). Phosphoric acid doped polybenzimidazole membrane for high temperature PEM fuel cell. Journal of Applied Polymer Science, 124(S1), E267–E277. https://doi.org/10.1002/app.36507

[26] **Litt, M., Ameri, R., Wang, Y., Savinell, R., & Wainwright, J.** (1998). Polybenzimidazoles/Phosphoric Acid Solid Polymer Electrolytes: Mechanical and Electrical Properties. MRS Proceedings, 548, 313–323. https://doi.org/10.1557/proc-548-313

[27] **Qu, T., Hu, J., Tan, Q., Liu, Y., Chen, Y., Sun, J., & Liu, Y.** (2021). Effect of phosphoric acid-doped polybenzimidazole membranes on the performance of H^+-ion concentration cell. International Journal of Hydrogen Energy, 46(5), 4354–4364. https://doi.org/10.1016/j.ijhydene.2020.10.223

[28] **Arslan, F., Böhm, T., Kerres, J., & Thiele, S.** (2021). Spatially and temporally resolved monitoring of doping polybenzimidazole membranes with phosphoric acid. Journal of Membrane Science, 625, 119145. https://doi.org/10.1016/j.memsci.2021.119145

[29] **Skorikova, G., Rauber, D., Aili, D., Martin, S., Li, Q., Henkensmeier, D., & Hempelmann, R.** (2020). Protic ionic liquids immobilized in phosphoric acid-doped polybenzimidazole matrix enable polymer electrolyte fuel cell operation at 200 °C. Journal of Membrane Science, 608, 118188. https://doi.org/10.1016/j.memsci.2020.118188

[30] **Wang, L., Liu, Z., Ni, J., Xu, M., Pan, C., Wang, D., Liu, D., & Wang, L.** (2019). Preparation and investigation of block polybenzimidazole membranes with high battery performance and low phosphoric acid doping for use in high-temperature fuel cells. Journal of Membrane Science, 572, 350–357. https://doi.org/10.1016/j.memsci.2018.10.083

[31] **Shogbon, C. B., Brousseau, J. L., Zhang, H., Benicewicz, B. C., & Akpalu, Y. A.** (2006). Determination of the Molecular Parameters and Studies of the Chain Conformation of Polybenzimidazole in DMAc/LiCl. Macromolecules, 39(26), 9409–9418. https://doi.org/10.1021/ma0609836

[32] **Jheng, L. C., Huang, C. Y., & Hsu, S. L. C.** (2013). Sulfonated MWNT and imidazole functionalized MWNT/polybenzimidazole composite membranes for high-temperature proton exchange membrane fuel cells. International Journal of Hydrogen Energy, 38(3), 1524–1534. https://doi.org/10.1016/j.ijhydene.2012.10.111

[33] **Kawahara, M., Morita, J., Rikukawa, M., Sanui, K., & Ogata, N.** (2000). Synthesis and proton conductivity of thermally stable polymer electrolyte: poly(benzimidazole) complexes with strong acid molecules. Electrochimica Acta, 45(8–9), 1395–1398. https://doi.org/10.1016 /s0013-4686(99)00349-7

[34] **Ma, Y. L., Wainright, J. S., Litt, M. H., & Savinell, R. F.** (2004). Conductivity of PBI Membranes for High-Temperature Polymer Electrolyte Fuel Cells. Journal of The Electrochemical Society, 151(1), A8. https://doi.org/ 10.1149/1.1630037

[35] **Iqbal, H., Bhowmik, S., & Benedictus, R.** (2019). Durability of PBI adhesive bonded joints under various environmental conditions. International Journal of Adhesion and Adhesives, 89, 154–160. https://doi.org/ 10.1016/j.ijadhadh.2019.01.006

[36] **High Performance Thermoplastic Polymers | Celazole® PBI Polymer.** (2020, February 11). Celazole® PBI. https://pbipolymer.com/celazole-pbi-products/ Last Access: 13.07.2021

[37] **Mark, H. F., & Bikales, N. M.** (2004). Encyclopedia of Polymer Science and Technology (12 Volume Set) (3rd Edition, 12 Volume Set ed., Vol. 11). Wiley-Interscience.

[38] **Yang, J., Liu, C., Gao, L., Wang, J., Xu, Y., & He, R.** (2015). Novel composite membranes of triazole modified graphene oxide and polybenzimidazole for high temperature polymer electrolyte membrane fuel cell applications. RSC Advances, 5(122), 101049–101054. https://doi.org/ 10.1039/c5ra16554g

[39] **Cai, Y., Yue, Z., Teng, X., & Xu, S.** (2018). Radiation grafting graphene oxide reinforced polybenzimidazole membrane with a sandwich structure for high temperature proton exchange membrane fuel cells in anhydrous atmosphere. European Polymer Journal, 103, 207–213. https://doi.org/ 10.1016/j.eurpolymj.2018.02.020

[40] **Bayer, T., Selyanchyn, R., Fujikawa, S., Sasaki, K., & Lyth, S.** (2017). Spray-painted graphene oxide membrane fuel cells. Journal of Membrane Science, 541, 347–357. https://doi.org/10.1016/j.memsci.2017.07.012

[41] **Üregen, N., Pehlivanoğlu, K., Özdemir, Y., & Devrim, Y.** (2017). Development of polybenzimidazole/graphene oxide composite membranes for high temperature PEM fuel cells. International Journal of Hydrogen Energy, 42(4), 2636–2647. https://doi.org/10.1016/j.ijhydene.2016.07.009

[42] **Deng, Y., Wang, G., Fei, M. M., Huang, X., Cheng, J., Liu, X., Xing, L., Scott, K., & Xu, C.** (2016). A polybenzimidazole/graphite oxide based three layer membrane for intermediate temperature polymer electrolyte membrane fuel cells. RSC Advances, 6(76), 72224–72229. https://doi.org/10.1039/c6ra11307a

[43] **Xu, C., Liu, X., Cheng, J., & Scott, K.** (2015). A polybenzimidazole/ionic-liquid-graphite-oxide composite membrane for high temperature polymer electrolyte membrane fuel cells. Journal of Power Sources, 274, 922–927. https://doi.org/10.1016/j.jpowsour.2014.10.134

[44] **Paneri, A., Heo, Y., Ehlert, G., Cottrill, A., Sodano, H., Pintauro, P., & Moghaddam, S.** (2014). Proton selective ionic graphene-based membrane for high concentration direct methanol fuel cells. Journal of Membrane Science, 467, 217–225. https://doi.org/10.1016/j.memsci.2014.05.002

[45] **Xu, C., Cao, Y., Kumar, R., Wu, X., Wang, X., & Scott, K.** (2011). A polybenzimidazole/sulfonated graphite oxide composite membrane for high temperature polymer electrolyte membrane fuel cells. Journal of Materials Chemistry, 21(30), 11359. https://doi.org/10.1039/c1jm11159k

[46] **Yang, J., Liu, C., Gao, L., Wang, J., Xu, Y., & He, R.** (2015b). Novel composite membranes of triazole modified graphene oxide and polybenzimidazole for high temperature polymer electrolyte membrane fuel cell applications. RSC Advances, 5(122), 101049–101054. https://doi.org/10.1039/c5ra16554g

[47] **Guerrero Moreno, N., Gervasio, D., Godínez García, A., & Pérez Robles, J. F.** (2015). Polybenzimidazole-multiwall carbon nanotubes composite membranes for polymer electrolyte membrane fuel cells. Journal of Power Sources, 300, 229–237. https://doi.org/10.1016/j.jpowsour.2015.09.070

[48] **Wu, J. F., Lo, C. F., Li, L. Y., Li, H. Y., Chang, C. M., Liao, K. S., Hu, C. C., Liu, Y. L., & Lue, S. J.** (2014). Thermally stable polybenzimidazole/carbon nano-tube composites for alkaline direct methanol fuel cell applications. Journal of Power Sources, 246, 39–48. https://doi.org/10.1016/j.jpowsour.2013.05.171

[49] **Suryani, Chang, C. M., Liu, Y. L., & Lee, Y. M.** (2011). Polybenzimidazole membranes modified with polyelectrolyte-functionalized multiwalled carbon nanotubes for proton exchange membrane fuel cells. Journal of Materials Chemistry, 21(20), 7480. https://doi.org/10.1039/c1jm10439j

[50] **Kannan, R., Kagalwala, H. N., Chaudhari, H. D., Kharul, U. K., Kurungot, S., & Pillai, V. K.** (2011). Improved performance of phosphonated carbon nanotube–polybenzimidazole composite membranes in proton exchange membrane fuel cells. Journal of Materials Chemistry, 21(20), 7223. https://doi.org/10.1039/c0jm04265j

[51] **Shao, H., Shi, Z., Fang, J., & Yin, J.** (2009). One pot synthesis of multiwalled carbon nanotubes reinforced polybenzimidazole hybrids: Preparation, characterization and properties. Polymer, 50(25), 5987–5995. https://doi.org/10.1016/j.polymer.2009.10.044

[52] **Yuan, X., Song, C., Wang, H., & Zhang, J.** (2014). Electrochemical Impedance Spectroscopy in PEM Fuel Cells: Fundamentals and Applications (2010th ed.). Springer.

[53] **Soboleva, T., Xie, Z., Shi, Z., Tsang, E., Navessin, T., & Holdcroft, S.** (2008). Investigation of the through-plane impedance technique for evaluation of anisotropy of proton conducting polymer membranes. Journal of Electroanalytical Chemistry, 622(2), 145–152. https://doi.org/10.1016/j.jelechem.2008.05.017

[54] **Li, Q., Aili, D., Hjuler, H. A., & Jensen, J. O.** (2015). High Temperature Polymer Electrolyte Membrane Fuel Cells: Approaches, Status, and Perspectives (1st ed. 2016 ed.). Springer.

[55] **Li, X., Qian, G., Chen, X., & Benicewicz, B. C.** (2013). Synthesis and Characterization of a New Fluorine-Containing Polybenzimidazole (PBI) for Proton-Conducting Membranes in Fuel Cells. Fuel Cells, n/a. https://doi.org/10.1002/fuce.201300054

[56] **Eren, E. O., Özkan, N., & Devrim, Y.** (2020b). Polybenzimidazole-modified carbon nanotubes as a support material for platinum-based high-temperature proton exchange membrane fuel cell electrocatalysts. International Journal of Hydrogen Energy. Published. https://doi.org/10.1016/j.ijhydene.2020.07.101

[57] **Li, Q.** (2004). Water uptake and acid doping of polybenzimidazoles as electrolyte membranes for fuel cells. Solid State Ionics, 168(1–2), 177–185. https://doi.org/10.1016/j.ssi.2004.02.013

[58] **Xie, Z., Song, C., Andreaus, B., Navessin, T., Shi, Z., Zhang, J., & Holdcroft, S.** (2006). Discrepancies in the Measurement of Ionic Conductivity of PEMs Using Two- and Four-Probe AC Impedance Spectroscopy. Journal of The Electrochemical Society, 153(10), E173. https://doi.org/10.1149/1.2258091

[59] **Xu, G., Wei, Z., Li, S., Li, J., Yang, Z., & Grigoriev, S. A.** (2019). In-situ sulfonation of targeted silica-filled Nafion for high-temperature PEM fuel cell application. International Journal of Hydrogen Energy, 44(56), 29711–29716. https://doi.org/10.1016/j.ijhydene.2019.02.037

[60] **Xu, G., Wu, Z., Wei, Z., Zhang, W., Wu, J., Li, Y., Li, J., Qu, K., & Cai, W.** (2020). Non-destructive fabrication of Nafion/silica composite membrane via swelling-filling modification strategy for high temperature and low humidity PEM fuel cell. Renewable Energy, 153, 935–939. https://doi.org/10.1016/j.renene.2020.02.056

CURRICULUM VITAE

Name Surname **:** Mehmet Turan GÖRÜRYILMAZ

EDUCATION

- **B.Sc.** **:** 2017, Gazi University, Faculty of Engineering, Department of Mechanical Engineering

PROFESSIONAL EXPERIENCE AND REWARDS:

- Research Assistant, Turkish – German University, Faculty of Science, Energy Science and Technologies